# OH Roaming and Beyond in the Unimolecular Decay of the Methyl-Ethyl Substituted Criegee Intermediate: Observations and Predictions

Tianlin Liu<sup>a</sup>, Sarah N. Elliott<sup>b</sup>, Meijun Zou<sup>a</sup>, Michael F. Vansco<sup>b</sup>, Christopher A. Sojdak<sup>a</sup>, Charles R. Markus<sup>c,d</sup>, Raybel Almeida<sup>e</sup>, Kendrew Au<sup>e</sup>, Leonid Sheps<sup>e</sup>, David L. Osborn<sup>e,f</sup>, Frank A. F. Winiberg<sup>c</sup>, Carl J. Percival<sup>c</sup>, Craig A. Taatjes<sup>e</sup>, Rebecca L. Caravan<sup>b</sup>, Stephen J. Klippenstein<sup>b,\*</sup>, and Marsha I. Lester<sup>a,\*</sup>

#### Abstract

Alkene ozonolysis generates short-lived Criegee intermediates, which are a significant source of hydroxyl (OH) radicals. This study demonstrates that roaming of the separating OH radicals can yield alternate hydroxycarbonyl products, thereby reducing the OH yield. Specifically, hydroxybutanone has been detected as a stable product arising from roaming in the unimolecular decay of the methyl-ethyl substituted Criegee intermediate (MECI) under thermal flow cell conditions. The dynamical features of this novel multistage dissociation plus roaming unimolecular decay process have also been examined with ab initio kinetics calculations. Experimentally, hydroxybutanone isomers are distinguished from isomeric MECI by their higher ionization threshold and distinctive photoionization spectra. Moreover, the exponential rise of the hydroxybutanone kinetic time profile matches that for unimolecular decay of MECI. A weaker methyl vinyl ketone (MVK) photoionization signal is also attributed to OH roaming. Complementary multireference electronic structure calculations have been utilized to map the unimolecular decay pathways for MECI, starting with 1,4 H-atom transfer from a methyl or methylene group to the terminal oxygen, followed by roaming of the separating OH and butanonyl radicals in the long-range region of the potential. Roaming via reorientation and addition of OH to the vinyl group of butanonyl is shown to yield hydroxybutanone, and subsequent C-O elongation and H-transfer can lead to MVK. A comprehensive theoretical kinetic analysis has been conducted to evaluate rate constants and branching yields (ca. 10-11%) for thermal unimolecular decay of MECI to conventional and roaming products under laboratory and atmospheric conditions, consistent with the estimated experimental yield (ca. 7%).

<sup>&</sup>lt;sup>a</sup> Department of Chemistry, University of Pennsylvania, Philadelphia, PA 19104-6323, USA.

<sup>&</sup>lt;sup>b</sup> Chemical Sciences and Engineering Division, Argonne National Laboratory, Lemont, IL 60439, USA.

<sup>&</sup>lt;sup>e</sup> NASA Jet Propulsion Laboratory, California Institute of Technology, 4800 Oak Grove Drive, Pasadena, CA 91109, USA.

<sup>&</sup>lt;sup>d</sup> Division of Chemistry and Chemical Engineering, California Institute of Technology, Pasadena, CA 91125, USA

<sup>&</sup>lt;sup>e</sup> Combustion Research Facility, Mailstop 9055, Sandia National Laboratories, Livermore, CA 94551, USA.

Department of Chemical Engineering, University of California, Davis, CA 95616, USA

<sup>\*</sup> Corresponding author emails: milester@sas.upenn.edu, sik@anl.gov

#### A. Introduction

Alkenes are emitted into Earth's troposphere from both anthropogenic and biogenic sources. Ozonolysis is a significant removal pathway of alkenes, which generates short-lived, highly reactive carbonyl oxide intermediates (R<sub>1</sub>R<sub>2</sub>C=O<sup>+</sup>O<sup>-</sup>), known as Criegee intermediates. <sup>1-2</sup> Alkene ozonolysis proceeds via cycloaddition of ozone across a C=C bond of the alkene, forming a primary ozonide, which decomposes in a highly exothermic process to yield internally excited Criegee intermediates. The excited Criegee intermediates may undergo prompt unimolecular decay via several possible mechanisms, producing hydroxyl (OH) radicals and other products. Alternatively, the Criegee intermediates can be collisionally stabilized and decay by thermal unimolecular dissociation and/or bimolecular reaction with other atmospheric species including H<sub>2</sub>O, SO<sub>2</sub>, NO<sub>x</sub>, and organic acids.<sup>3</sup> The unimolecular decay of both internally excited and thermalized Criegee intermediates is an important non-photolytic source of OH radicals, 1-2 a key atmospheric oxidant that initiates the breakdown of many trace species. This pathway is a particularly important source of OH at nighttime and during the winter when the dominant ozone photolysis production is inhibited. However, analysis of measurements recorded during the PUMA field campaign in the West Midlands, UK have indicated that Criegee intermediates decomposition may contribute substantially to measured summer daytime OH (46%, cf. 62% in winter daytime)<sup>4</sup> in certain environments. Bimolecular reactions of Criegee intermediates can lead to functionalized hydroperoxides and aerosol precursors. The rates and relative atmospheric importance and impact of these various removal pathways depend on the substituents (e.g. R<sub>1</sub>, R<sub>2</sub> = H, methyl, ethyl, and/or vinyl groups) and conformational form of the Criegee intermediates.<sup>3, 5-8</sup>

Unimolecular decay of alkyl-substituted Criegee intermediates generally proceeds via intramolecular 1,4 H-atom transfer from an alkyl group to the terminal O-atom, transiently forming a vinyl hydroperoxide (VHP), followed by O-O bond fission that releases hydroxyl (OH) and vinoxy radicals. 5-6 While unimolecular decay of Criegee intermediates to OH products can occur promptly or following thermalization, recent experimental and theoretical studies suggest that roaming may also be operative. 9-11 Roaming occurs in unimolecular reactions when a vibrationally energized molecule, heading for dissociation into fragments by simple bond fission, leads instead to reorientation of the fragments in the long range (3-8 Å) region of the potential and an alternative intra-fragment reaction (e.g. addition or abstraction) yields distinctly different products from conventional unimolecular decomposition mechanisms. 12-14 In the unimolecular decay of Criegee intermediates, O-O bond elongation leads to long-range regions of the potential where the separating OH radical can reorient, roam, and add to the vinyl group, resulting in roaming-induced isomerization to hydroxycarbonyl products. This study explores a wide range of intra-fragment roaming reactions, involving both addition and abstraction pathways, which can occur in the unimolecular decay of thermalized Criegee intermediates, and reports their yield under

both laboratory and atmospheric thermal conditions. The combination of experimental observation and theoretical analyses is used to obtain a uniquely well validated and quantified description of the detailed dynamics and kinetics of roaming in a thermal system.

One such hydroxycarbonyl, hydroxyacetone [CH<sub>3</sub>C(O)CH<sub>2</sub>OH], was detected as an end product in early ozonolysis studies of tetramethylethylene. <sup>15-16</sup> A more recent direct study of the acetone oxide Criegee intermediate [(CH<sub>3</sub>)<sub>2</sub>COO], generated photolytically, <sup>17</sup> identified hydroxyacetone as a stable isomeric product using tunable vacuum ultraviolet (VUV) photoionization mass spectrometry. A companion theoretical study identified two unimolecular decay pathways for (CH<sub>3</sub>)<sub>2</sub>COO following 1,4 H-atom transfer to VHP: simple O-O bond fission to OH + vinoxy products and an alternative isomerization pathway involving intramolecular OH migration to the terminal CH<sub>2</sub> group producing hydroxyacetone. A subsequent theoretical study identified a lower energy OH migration as a roaming radical mechanism with steering of the OH moiety to the α carbon due to hydrogen bonding. 10 A related statistical rate study predicted that the yield of hydroxyacetone will be significantly enhanced at lower temperatures (> 50% yield at 200 K vs. ca. 10% at 298 K), but relatively insensitive to pressure ( $\le 1$ bar). 10 An analogous OH roaming reaction pathway has recently been predicted for unimolecular decay of methyl vinyl ketone oxide, a four-carbon unsaturated Criegee intermediate formed from isoprene ozonolysis.<sup>11</sup> Earlier theoretical studies of CH<sub>3</sub>CHOO unimolecular decay had shown that O-O bond cleavage of the associated vinyl hydroperoxide (CH<sub>2</sub>CHOOH) is not a simple, barrierless O-O bond breaking process, but rather involves a submerged saddle point and associated shallow minimum in the exit channel. 18-19

The present study examines unimolecular decay pathways for the methyl-ethyl substituted Criegee intermediate [MECI, (CH<sub>3</sub>)(CH<sub>3</sub>CH<sub>2</sub>)COO], which is a prototypical Criegee intermediate arising from the ozonolysis of 3,4-dimethyl-3-hexene<sup>20-21</sup> and other branched, asymmetric alkenes. MECI exists in two distinct groups of conformational forms that differ by the orientation of the carbonyl oxide group, which may be oriented either towards the methyl (*anti*, *E*) or the ethyl (*syn*, *Z*) substituent and have similar ground state stabilities (within 1 kcal mol<sup>-1</sup>).<sup>22</sup> The *anti* and *syn* conformers are separated by significant barriers (~37 kcal mol<sup>-1</sup>) associated with internal rotation about the C=O bond,<sup>22-23</sup> and are considered as separate species under thermal conditions. In each case, the ethyl substituent has two orientations that can rapidly interconvert by internal rotation about a C-C bond under thermal conditions.<sup>22,24</sup> MECI was initially observed and structurally characterized by Fourier transform microwave spectroscopy (FTMW) under jet-cooled conditions, following production in a pulsed electric discharge of 2,2-diiodobutane precursor and O<sub>2</sub>,<sup>24</sup> and later separately investigated by IR and UV spectroscopic methods under similar jet-cooled conditions utilizing 248 nm photolysis of the precursor.<sup>22,25</sup>

As shown in Scheme 1, both *anti*- and *syn*-conformers of MECI can readily undergo unimolecular decay by 1,4 H-atom transfer mechanisms. The H-atom transfers from a methyl group (R'=H) or methylene group (R'=CH<sub>3</sub>) for *anti*- and *syn*-conformers, respectively, to the terminal oxygen via 5-membered ring transition states (TS) to form vinyl hydroperoxide, specifically hydroperoxybutene (HPB), intermediates. In the conventional unimolecular decay mechanism, HPB would then decompose by prompt O-O bond cleavage to form vinoxy, in this case butanonyl, and OH radical products.

Scheme 1. Conventional 1,4 H-atom transfer mechanism for unimolecular decay of *anti*-MECI (R=CH<sub>2</sub>CH<sub>3</sub>, R'=H) or *syn*-MECI (R=CH<sub>3</sub>, R'= CH<sub>3</sub>) conformers proceeds via 5-membered ring transition states (TS) and hydroperoxybutene (HPB) intermediates to butanonyl + OH radical products.

The unimolecular decay dynamics of jet-cooled MECI have been investigated by IR activation in the overtone CH stretch (2v<sub>CH</sub>) region with time-resolved, laser-induced fluorescence (LIF) detection of the OH products.<sup>22</sup> This provided the rate of appearance of OH products at excitation energies in the vicinity of the TS barrier and, equivalently, energy-dependent unimolecular decay rates k(E) for MECI. Both anti- and syn-MECI can undergo 1,4 H-atom transfer reactions, but proceed via different transition state (TS) barriers. High-level electronic structure calculations predicted a TS barrier for anti-MECI of 16.1 kcal mol<sup>-1</sup> (TS<sub>anti</sub>, relative to anti1-MECI) and that for syn-MECI of 15.4 kcal mol<sup>-1</sup> (TS<sub>syn</sub>, relative to syn1-MECI).<sup>22</sup> The experimental energy-dependent rate measurements were in good accord with statistical RRKM calculations based on the computed TS barriers and accounting for quantum mechanical tunneling. Master equation modeling was then utilized to predict the thermal unimolecular decay rate k(T, P) at 298 K (1 bar) for anti-MECI of 473 s<sup>-1</sup> and a more rapid thermal decay rate for syn-MECI of 660 s<sup>-1</sup> due to its lower TS barrier.<sup>22</sup> Other features of the computed reaction coordinates differed. In particular, the OH + 2-butanone-1-yl product asymptote was predicted to lie 3.9 kcal mol<sup>-1</sup> higher in energy than anti-MECI, while the OH + 2-butanone-3-yl product asymptote was nearly isoenergetic with syn-MECI. In this work, unlike the prior study, <sup>22</sup> energies are referenced to the OH + butanonyl product asymptotes, rather than the anti- or syn-MECI reactants.

The present study demonstrates that unimolecular decay of *anti*- and *syn*-MECI under thermal conditions can also proceed via roaming mechanisms, yielding stable hydroxybutanone [CH<sub>3</sub>CH<sub>2</sub>C(O)CH<sub>2</sub>OH (1H2B) or CH<sub>3</sub>CH(OH)C(O)CH<sub>3</sub> (3H2B)] and other products, which are detected using tunable VUV photoionization with mass- and kinetic time-resolution. Complementary theoretical

calculations reveal many roaming pathways and products, including isomerization to hydroxybutanone, which can occur in the unimolecular decay of *anti*- and *syn*-MECI under analogous thermal conditions. Also, a novel roaming induced abstraction channel is shown to result from direct molecular elimination of water from the hydroxybutanone. In addition, a theoretical kinetic analysis predicts the yield of products resulting from conventional and roaming pathways in the thermal unimolecular decay of MECI over a wide range of temperature (200-350 K) and pressure (0.001 to 1 bar) conditions, including temperature-pressure conditions of relevance to the troposphere. The present calculations focus on the thermal unimolecular decay of MECI employing multireference methods to examine the roaming aspects of the potential energy surface and state-of-the-art transition state theory methods to predict the kinetics, thereby providing a much firmer foundation to prior theoretical suggestions<sup>9-10</sup> of the role of roaming in Criegee intermediate dissociation.

#### B. Methods

# 1. Experimental Methods

Experiments were carried out using the Sandia Multiplexed Photoionization Mass Spectrometer (MPIMS) apparatus interfaced with the tunable VUV radiation of the Chemical Dynamics Beamline (9.0.2) at the Advanced Light Source (Lawrence Berkeley National Laboratory).<sup>26</sup> The 2,2-diidobutane [CH<sub>3</sub>CH<sub>2</sub>(CH<sub>3</sub>)CI<sub>2</sub>] precursor for photolytic production of MECI was synthesized as described in Refs. 22 and 27. The vapor of the 2,2-diidobutane precursor (0.19 Torr at 298 K)<sup>28</sup> was entrained into a flow of He using a temperature- and pressure-regulated glass bubbler (298 K, 650 Torr), then mixed with O<sub>2</sub> and He bath gas via calibrated mass flow controllers. The gas mixture was delivered to a slow-flow quartz reactor (10 Torr, 298 K) coated with halocarbon wax. An excimer laser operating at 248 nm (KrF excimer laser, 10 Hz, ~0.5 W) was propagated along the length of the flow tube to generate methyl-ethyl substituted Criegee intermediates (MECI) via photolysis of the precursor and subsequent reaction of the resultant mono-iodo radical with excess O<sub>2</sub>.<sup>22</sup> The concentration of MECI produced was varied by attenuating the laser output (by 50% or 75%) with fine meshes. A continuous, nearly effusive flow of gas passed through an orifice (300 or 650 µm) in the side of the reactor tube, and the resultant molecular beam was skimmed and intercepted with the VUV radiation. The resultant photoions were pulse extracted and detected utilizing an orthogonally accelerated time-of-flight mass spectrometer with mass resolution (m/ $\Delta$ m) of approximately 1000.

Three-dimensional data sets (m/z, kinetic time, photoionization energy) were recorded by collecting time-resolved mass spectra while stepping the photoionization energy from 8.3 to 11.0 eV in 0.05 eV increments. These three-dimensional datasets were utilized to identify and resolve reactants, intermediates, and products via their characteristic photoionization spectra. A larger number of laser

shots were averaged to obtain kinetic time profiles with higher signal-to-noise (S/N) at fixed photoionization energies of 8.9, 9.3, 9.7, and 10.5 eV.

The photoionization spectra of 1-hydroxy-2-butanone (1H2B) and 3-hydroxy-2-butanone (3H2B) (Sigma-Aldrich) were separately recorded from 9.3-11 eV in 0.05 eV increments using that of propene as a calibration standard,<sup>29</sup> according to the method described by Welz et al.<sup>30</sup> The absolute photoionization spectrum for 1H2B was established utilizing its vapor pressure; 3H2B (acetoin) may dimerize and/or crystallize, resulting in an inexact concentration that precludes determination of its absolute cross section. The absolute photoionization spectra for other species were adopted from prior studies.<sup>30-35</sup>

In some experiments, SO<sub>2</sub> was added as a scavenger gas for Criegee intermediates. Single-energy experiments (9.7 eV) were performed at various SO<sub>2</sub> concentrations to evaluate changes in the amount of potential unimolecular products. For these experiments, SO<sub>2</sub> was diluted with He and added to the gas mixture via a calibrated mass controller.

#### 2. Theoretical Methods

The adiabatic ionization energies (AIE) of MECI, hydroperoxybutene (HPB-1 or HPB-2), and hydroxybutanone (1H2B or 3H2B) isomers were computed at the CCSD(T)-F12b/aug-cc-pVTZ/B2PLYP-D3/cc-pVTZ level of theory, including harmonic zero-point energy (ZPE) corrections (Table SE1). Franck-Condon factor (FCF) calculations associated with photoionization of MECI were carried out utilizing the ezFCF v1.2 code.<sup>36-37</sup> Energies along reaction pathways involving roaming to hydroxybutanone and other products, along with C-C bond fission of hydroxybutanone, were evaluated with multireference methods (Table ST1). Stationary point energies associated with the conventional 1,4 H-atom transfer mechanism for *anti*- and *syn*-MECI to OH + butanonyl radical products were adopted from prior work of Barber et al. using ANL0-B2F [CCSD(T)-F12/CBS-F12(TZ-F12,QZ-F12)//B2PLYP-D2/cc-pVTZ + corrections] (Table ST2).<sup>22</sup> The stationary point energies for the stable products of these roaming reactions and for a set of tight TS to produce methyl vinyl ketone + H<sub>2</sub>O from 3H2B were also evaluated using the ANL0-B2F method (Table ST2).

Supporting information and associated Tables and Figures are denoted as SE and ST for supporting experimental and theoretical information, respectively.

#### C. Experimental Results

A prior study focused on the 1,4 H-atom transfer pathway from IR-activated MECI to vinyl hydroperoxide (HPB), followed by prompt O-O bond dissociation to form OH + butanonyl products under jet-cooled, collision-free conditions.<sup>22</sup> Recent experimental and theoretical studies of other Criegee intermediates have suggested that unimolecular decay of Criegee intermediates under atmospheric temperature and pressure conditions may lead to additional products via roaming pathways.<sup>9-11</sup> The

present study focuses on identification of roaming pathways for MECI under thermal conditions (298 K), consisting of isomerization of MECI to a vinyl hydroperoxide (HPB-1 or HPB-2), OH roaming from the hydroperoxide group toward the vinyl group, and generation of hydroxybutanone (1H2B or 3H2B) and/or other products.

# 1. Identification of hydroxybutanone products

Hydroxybutanone (1H2B and/or 3H2B) products formed from OH roaming pathways are isomers of MECI and vinyl hydroperoxide (HPB-1 and HPB-2) with the same mass (m/z 88). Nevertheless, hydroxybutanone products are identified in the present experimental study based on their higher photoionization energy thresholds and persistent signal at long kinetic times indicative of stable products. The AIE predicted for hydroxybutanone products (1H2B of 9.2 eV and 3H2B of 9.4 eV) are at least ca. 0.5 eV higher than those computed for the MECI Criegee intermediates (8.7 eV). They are also higher than those anticipated for vinyl hydroperoxides (HPB-1 and HPB-2 of 8.7 and 8.3 eV, respectively). The AIE calculations are summarized in Table SE1.

The production of MECI conformers and their unimolecular decay products were identified using MPIMS via a combination of high-resolution time-of-fight mass spectrometry, kinetic temporal profiles, and photoionization scans.<sup>26</sup> A Gaussian fit of the m/z 88 signal yielded a mass of 88.052  $\pm$  0.002 amu (Figure SE1), consistent with the exact mass of MECI (88.053 amu) and its isomers. The kinetic temporal profiles associated with m/z 88 upon photoionization at 8.9 and 9.7 eV show a prompt rise resulting from photolytic production of MECI, followed by a rapid decay attributed to thermal unimolecular decay and potentially a small contribution from bimolecular or wall loss as shown in Figure 1. The rapid decay of the m/z 88 signal at 8.9 eV, ca.  $510 \pm 40 \text{ s}^{-1} (\pm 2\sigma)$ , is consistent with the computed thermal unimolecular decay rates for *anti*- and/or *syn*-MECI (Table ST3). At 9.7 eV, a persistent non-zero photoionization signal is observed at long times, which is attributed to formation of a stable isomeric product at the same mass (m/z 88). At 8.9 eV, the photoionization signal lacks a significant long-time component; the small residual signal at long times may originate from other isomers not identified in this study.<sup>38</sup>

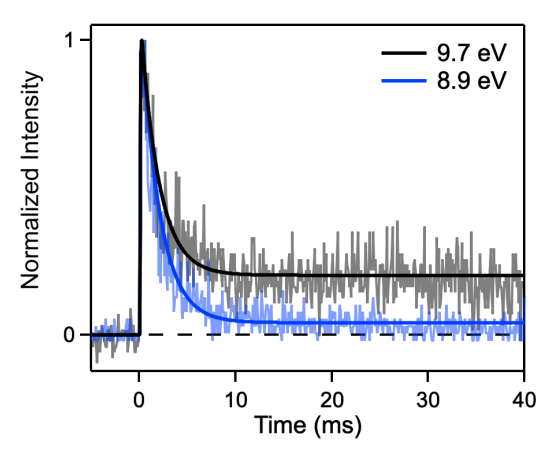


Figure 1. Kinetic time profiles of the m/z 88 channel observed upon photoionization at 8.9 eV (blue) and 9.7 eV (black) following photolytic production of MECI. The m/z 88 signals exhibit a prompt rise followed by a rapid decay to a persistent non-zero signal (9.7 eV) or near baseline (8.9 eV). The rapid decay of the m/z 88 signal is attributed primarily to thermal unimolecular decay of MECI.

Photoionization spectra of the m/z 88 mass channel components were obtained from 8.3 to 11.0 eV by integrating over early 0-5 ms and later 10-40 ms times after photolytic production of MECI, as shown in Figure 2. The early time (0-5 ms) signal shows an onset at ca. 8.7 eV, which agrees with the computed adiabatic ionization energies for *syn* and *anti* conformers of MECI at ca. 8.7 eV (Table SE1). The early time photoionization signal also exhibits a second rise at ca. 9.8 eV. At later time (10-40 ms), the photoionization spectrum shows a distinct threshold at ca. 9.5 eV, in accord with the computed adiabatic ionization energies for hydroxybutanone (Table SE1). At later time (10-40 ms), the lower energy feature is not observed, consistent with unimolecular decay (and possible bimolecular or wall loss) of MECI. We note that the m/z 88 signal at long kinetic time (10-40 ms) scales linearly with excimer photolysis power (Figure SE2).<sup>9</sup>

Comparison with the photoionization spectra separately recorded for 1-hydroxy-2-butanone (1H2B, blue) and 3-hydroxy-2-butanone (3H2B, red) demonstrates that the long-time signal with threshold at ca. 9.5 eV is due to stable hydroxybutanone products. Least-squares fit of the experimental m/z 88 data to the absolute photoionization spectrum of 1H2B (blue) shows excellent agreement with uncertainties of  $\pm 1\sigma$  (dark gray) and  $\pm 2\sigma$  (light gray) indicated by shading. The photoionization spectrum separately recorded for 3-hydroxy-2-butanone (3H2B, red) shows a similar onset and shape, and thus the photoionization spectrum observed upon photolytic production of MECI likely has contributions from both 1H2B and 3H2B.

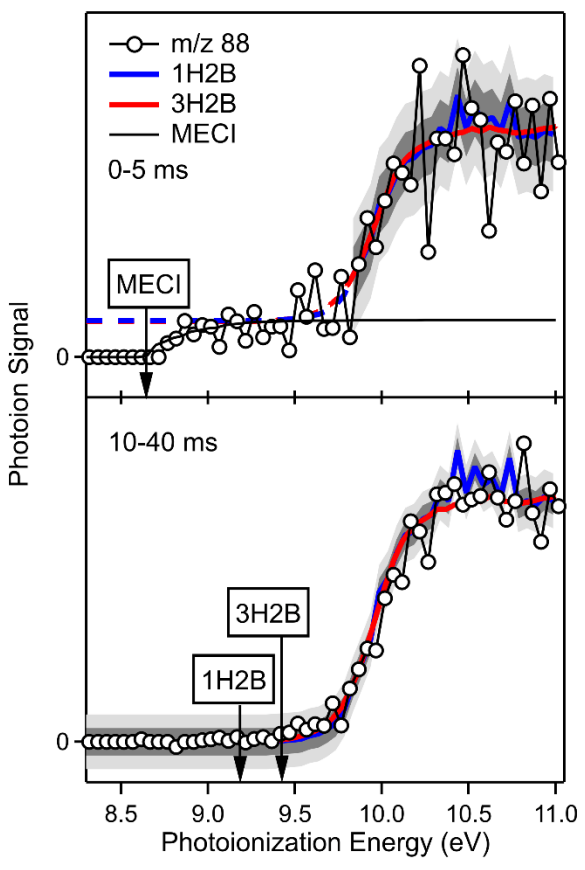


Figure 2. Photoionization spectra on the m/z 88 mass channel (open circles) integrated over early (0-5 ms) and later (10-40 ms) times after photolysis. The onset and shape of the photoionization spectrum obtained at later times are consistent with the photoionization spectra separately recorded for 1-hydroxy-2-butanone (1H2B, Table SE2) and 3-hydroxy-2-butanone (3H2B). The early-time spectrum obtained over the 9.8-11.0 eV energy region is also in good accord with those for 1H2B and 3H2B. Least-squares fit of the experimental m/z 88 data to the absolute photoionization spectrum of 1H2B (blue) shows excellent agreement with uncertainties of  $\pm 1\sigma$  (dark gray) and  $\pm 2\sigma$  (light gray) indicated by shading. The photoion signals are normalized by the photocurrent at each photon energy; the early and later time photoion signals are arbitrarily scaled for comparison. The computed adiabatic ionization energies for MECI and hydroxybutanone are indicated with arrows (see Table SE1).

The photoionization spectrum of MECI observed at early kinetic times (0-5 ms, Figure 2) is simulated by computing Franck-Condon factors<sup>36</sup> between the ground state of MECI and the lowest cationic state using the harmonic oscillator model, with allowance for Duschinsky rotation in the ezFCF code (see SE2),<sup>36-37</sup> as found for CH<sub>2</sub>OO and alkyl-substituted Criegee intermediates.<sup>9, 38-40</sup> The resultant simulation for *anti*- and *syn*-conformers of MECI (Figure SE3) shows that photoionization of MECI increases from its onset at ca. 8.7 eV to a constant contribution beyond ca. 9.8 eV (Figure 2).

The kinetic time profile for the hydroxybutanone product is also derived from the MPIMS data at m/z 88. A series of photoionization spectra are extracted over increasing time windows, in each case starting 5 ms prior to photolysis and sequentially increasing the integration time window. The photoionization spectra obtained over different time windows are integrated, after subtracting the constant MECI

photoionization signal from 9.75 to 11.0 eV, to obtain the total production of hydroxybutanone as a function of time. The gradient of the total production vs. time then yields the kinetic time profile for hydroxybutanone shown in Figure 3. The fitted rate of appearance for hydroxybutanone,  $410 \pm 110 \text{ s}^{-1}$  ( $\pm 2\sigma$ ), is in accord with the experimentally observed decay rate for MECI at 8.9 eV (Figure 1).

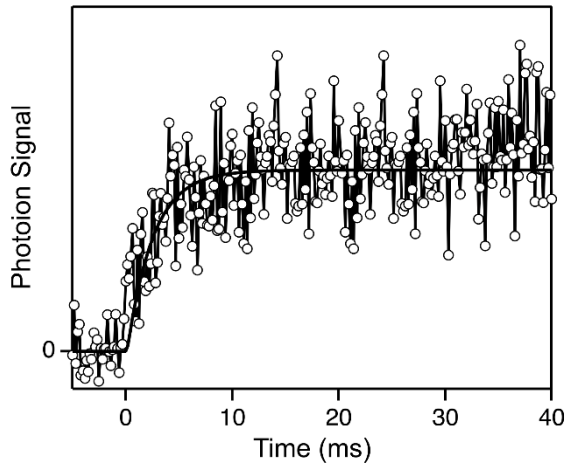


Figure 3. The kinetic time profile of the m/z 88 component selectively extracted at high photoionization energy (9.75-11.0 eV, open circles) reveals the temporal appearance of the hydroxybutanone (1H2B and/or 3H2B) products arising from OH roaming. The rate of appearance of hydroxybutanone (line) is in accord with the experimentally observed decay rate for MECI at 8.9 eV (Figure 1).

# 2. Scavenger Experiments

Additional experiments were conducted to verify the origin of the stable products observed on the m/z 88 mass channel at long kinetic times (10-40 ms). Kinetic time profiles were recorded with added SO<sub>2</sub> at 9.7 eV, where both MECI and hydroxybutanone are ionized (see Table SE1). The bimolecular reaction of MECI with SO<sub>2</sub> competes with the thermal unimolecular decay of MECI. The rate coefficient for bimolecular reaction of MECI with SO<sub>2</sub> has recently been determined [ $k_{SO_2} = 1.3 \pm 0.1 \times 10^{-10}$  cm<sup>3</sup> molecule<sup>-1</sup> s<sup>-1</sup> ( $\pm 2\sigma$ ), 10 Torr, 298 K]<sup>41</sup> and is expected to be similar for *anti*- and *syn*-MECI conformers. SO<sub>2</sub> was introduced at sufficient concentrations for its bimolecular reaction with MECI to compete with or exceed that associated with thermal unimolecular decay of MECI. The fraction (f) of m/z 88 signal remaining after addition of SO<sub>2</sub> at specific concentrations was measured as shown in Figure 4. These signals were integrated and normalized relative to the integrated m/z 88 signal without added SO<sub>2</sub>.

A simple kinetic model was utilized to predict the fraction (f) of m/z 88 signal that would remain with increasing bimolecular reaction with SO<sub>2</sub> according to:

$$f = \frac{k_{\text{uni}}}{k_{\text{uni}} + k_{\text{SO}_2} [\text{SO}_2]}$$

The simple model (dashed curves in Figure 4) agrees well with the experimentally observed change in the m/z 88 signal as a function of SO<sub>2</sub> concentration. A fit of the experimental data, assuming the same functional form as the kinetic model, yields  $k_{\text{uni}} = 470 \pm 80 \text{ s}^{-1} \ (\pm 2\sigma)$ . This is consistent with the thermal unimolecular decay rates predicted for *anti*- and *syn*-MECI under the experimental conditions of 330 and 494 s<sup>-1</sup> (Table ST3), respectively, which results in roaming to stable hydroxybutanone (m/z 88) and/or other products at long kinetic times.

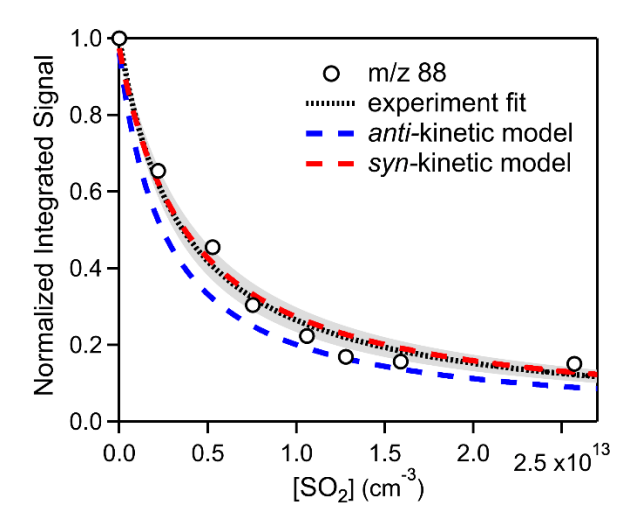


Figure 4. Integrated m/z 88 photoionization signal, recorded at 9.7 eV and long kinetic time (10-40 ms), as a function of added SO<sub>2</sub> concentration (points) and normalized to the signal without SO<sub>2</sub>. The experimental results are compared to a kinetic model that accounts for bimolecular reaction with SO<sub>2</sub> and thermal unimolecular decay of *anti*- and *syn*-MECI (blue and red dashed lines). A least squares fit of the experimental data (dotted line), assuming the functional form of the kinetic model, yields  $k_{uni} = 470 \pm 80$  s<sup>-1</sup> ( $\pm 2\sigma$ , gray shading) and extrapolates to zero at large [SO<sub>2</sub>].

# 3. Identification of other stable products

The MPIMS experiments also reveal formation of stable methyl vinyl ketone (MVK, m/z 70) products following photolytic generation of MECI. The kinetic appearance profile of the m/z 70 channel is consistent with the observed decay rate for MECI, and rises to a constant photoionization signal characteristic of a stable product as shown in Figure 5. A Gaussian fit of the m/z 70 signal yields an exact mass of  $70.043 \pm 0.003$  amu, in accord with the mass of MVK (70.042 amu). Finally, the onset and shape of the photoionization spectrum match those for MVK ( $9.65 \pm 0.02$  eV).  $^{34,42}$ 

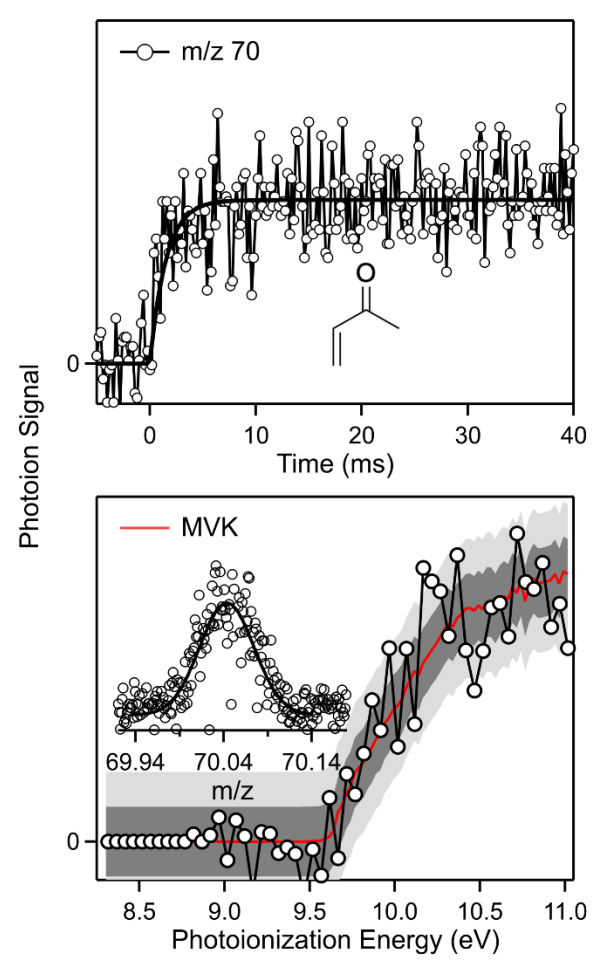


Figure 5. (Top) Kinetic temporal profile for appearance of the m/z 70 channel upon photoionization at 9.7 eV with rate constant similar to the thermal decay rate constant for MECI. (Inset) High resolution mass spectrum of the m/z 70 signal integrated over the full kinetic time window (0-40 ms). (Bottom) Photoionization spectrum obtained from 8.3 to 11.0 eV for m/z 70 integrated over the 10-40 ms kinetic time window. The red line shows the result of a least-squares fit of the absolute photoionization spectrum of methyl vinyl ketone to the experimental data with uncertainties in the fit of  $\pm 1\sigma$  (dark gray) and  $\pm 2\sigma$  (light gray) indicated by shading. The absolute photoionization spectrum of methyl vinyl ketone is adapted with permission from Ref. 34.

#### 4. Experimental yield of roaming products

The experimental yield of hydroxybutanone products is estimated as detailed in Sec. SE3. In brief, the concentrations of MECI and I-atoms are obtained from the photolytic depletion of the 2,2-diiodobutane ( $C_4H_8I_2$ ) precursor (ca. 6%), yielding an upper limit for the concentration of MECI of  $\leq 2.0 \times 10^{11}$  molecule cm<sup>-3</sup>. The concentration of hydroxybutanone is obtained by comparing its photoionization signals at 10.5 eV with that of I-atoms,<sup>43</sup> utilizing their absolute photoionization cross-sections.<sup>34, 44</sup> (The absolute photoionization cross section for 1H2B is separately determined in this work to be 6.8 Mb at 10.5 eV; the cross section for 3H2B is assumed to be similar to that for 1H2B.) As discussed in Sec. E, the theoretical kinetic yield is predicted to be much greater for 1H2B than 3H2B

under the present experimental conditions, such that the dominant roaming product is expected to be 1H2B. The resultant concentration of primarily 1H2B is estimated to be  $1.4 \times 10^{10}$  molecule cm<sup>-3</sup>, corresponding to a lower limit for its yield of ca. 7%. The MVK yield is at least an order of magnitude smaller than 1H2B (see Sec. SE3).

# 5. Fate of Radicals Generated in the Unimolecular Decay of MECI

The MPIMS experiments conducted under thermal conditions in a flow cell have resulted in detection of MECI, 1H2B and/or 3H2B, and MVK. Prior experiments carried out by IR activation of MECI under isolated, jet-cooled conditions selectively detected OH X <sup>2</sup>Π (v=0) products resulting from conventional O-O bond fission via UV LIF.<sup>22</sup> Photoionization detection of OH products was not pursued in the present study due to the high ionization energy (13.0 eV)<sup>45-46</sup> and reactivity of OH radicals. The butanonyl radicals generated in conventional unimolecular decay of *anti-* and *syn-*MECI are expected to react with excess O<sub>2</sub> in the flow cell and yield butanone peroxy radicals. As described in Sec. SE4, the butanone peroxy radicals can be stabilized, decompose to secondary products, and/or undergo bimolecular reactions including self-reaction. These processes yield products observed at m/z 86 and 71 (Figure SE5), which are consistent with diacetyl (or possibly 2-oxobutenal) and daughter ions of butanone peroxy radicals, respectively.

# D. Theoretical Analysis of Roaming Pathways

Theoretical investigation of the unimolecular decay of *anti*-MECI following 1,4 H-atom transfer to 2-hydroperoxy-but-1-ene (HPB-1) reveals that subsequent dissociation of HPB-1 is not a simple, barrierless bond cleavage reaction to OH + 2-butanone-1-yl radicals. Likewise, unimolecular decay of *syn*-MECI via 1,4 H-atom transfer to 2-hydroperoxy-but-2-ene (HPB-2) and subsequent evolution of HPB-2 toward OH + 2-butanone-3-yl radicals is predicted to be similarly complicated. In both cases, multi-reference theoretical methods reveal a complex potential energy landscape that can lead to additional products via roaming steps, involving reorientation of the radicals from one region of the long-range potential to another, followed by addition and/or abstraction pathways to yield final products. In the following discussions we choose reference energies that correlate with those of the separated fragments from the dissociation since that asymptote is a key factor in determining the branching in roaming radical reactions.

#### 1. Overview of Reaction Coordinates

An overview of the primary unimolecular decay pathways leading from the *anti*-conformer of MECI to products is shown in Figure 6. In this overview, energies are referenced to the OH + 2-butanone-1-yl product asymptote, rather than the *anti*-MECI reactant utilized in prior work.<sup>22</sup> Unimolecular decay of *anti*-MECI proceeds by 1,4 H-atom transfer from the methyl group to the terminal oxygen via TS<sub>anti</sub>,

forming 2-hydroperoxy-but-1-ene (HPB-1), followed by roaming of the OH and butanonyl radicals at long-range, which involves nearly thermoneutral passage through roaming TS and weakly bound complexes, each of which are submerged relative to OH + butanonyl. This decay can lead to conventional O'-O bond breakage and separation of the OH + 2-butanone-1-yl radical products in an endothermic process (3.9 kcal mol<sup>-1</sup>) or, alternatively, to the deep potential well of 1-hydroxy-2-butanone (1H2B) products. 1H2B can also undergo C1-C2 bond elongation and fission to separated hydroxymethyl (CH<sub>2</sub>OH) and propionyl (CH<sub>3</sub>CH<sub>2</sub>CO) radicals and/or lead to additional roaming pathways (not shown).

A Boltzmann distribution representing thermalized *anti*-MECI (298 K) in the present study is illustrated (blue). Tunneling through or passage over  $TS_{anti}$  yields the initial HPB-1 energy distribution (red), which is derived by scaling the *anti*-MECI thermal distribution with the tunneling-weighted unimolecular decay rates k(E) computed using statistical RRKM theory.<sup>22,47</sup> The initial HPB-1 distribution is peaked only ca. 10.6 kcal mol<sup>-1</sup> above the OH + 2-butanone-1-yl product asymptote, suggesting that thermal dissociation will be a dominant channel under the present experimental conditions, but also anticipating significant branching to 1H2B. Under atmospheric conditions, some portion of HPB-1 can be collisionally stabilized with an associated thermal distribution (blue) and/or undergo subsequent decay from a thermal distribution shown at the O'-O elongation TS (red).

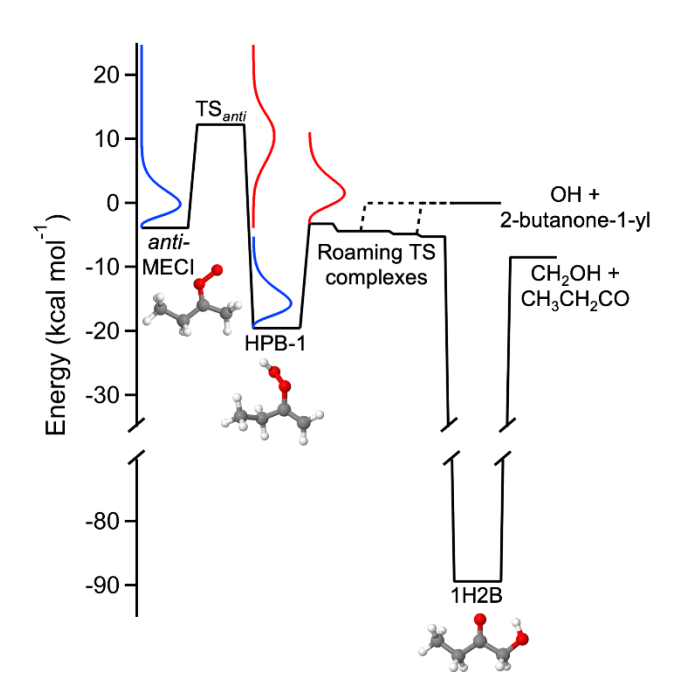


Figure 6. Reaction coordinate for the unimolecular pathways leading from the *anti*-conformer of MECI with energies relative to the OH + 2-butanone-1-yl product asymptote. Unimolecular decay proceeds via TS<sub>anti</sub> to 2-hydroperoxy-but-1-ene (HPB-1), followed by roaming of the separating OH and 2-butanone-1-yl radicals via roaming TS and complexes. This leads to OH + 2-butanone-1-yl radicals, 1-hydroxy-2-butanone (1H2B), and/or hydroxy methyl (CH<sub>2</sub>OH) + propionyl (CH<sub>3</sub>CH<sub>2</sub>CO) radical products.

Boltzmann distributions (298 K) for *anti*-MECI (blue), HPB-1 (blue), and at the first roaming TS (red) are illustrated. The initial HPB-1 distribution (red) is derived from the *anti*-MECI thermal distribution based on its energy-dependent unimolecular decay rates with tunneling.

An analogous overview of the primary unimolecular decay pathways for the *syn*-conformer of MECI to products is shown in Figure 7. Again, energies are referenced to the OH + 2-butanone-3-yl product asymptote, rather than the *syn*-MECI reactant utilized in prior work.<sup>22</sup> Unimolecular decay of *syn*-MECI proceeds by 1,4 H-atom transfer from the CH<sub>2</sub> group to the terminal oxygen via TS<sub>syn</sub>, forming 2-hydroperoxy-but-2-ene (HPB-2), followed by roaming of the OH and butanonyl radicals at long-range via submerged roaming TS and complexes. This decay can lead to conventional O'-O bond breakage and separation of the OH + 2-butanone-3-yl radical products in a nearly thermoneutral process or, alternatively, to the deep potential well of 3-hydroxy-2-butanone (3H2B) products. 3H2B can also undergo C2-C3 bond fission to separated hydroxyethyl (CH<sub>3</sub>CHOH) + acetyl (CH<sub>3</sub>CO) radicals, proceed via a deeply submerged barrier (TS<sub>water-elim</sub>) to eliminate water and form methyl vinyl ketone (MVK), and/or lead to additional roaming pathways (not shown).

A Boltzmann distribution representing thermalized *syn*-MECI (298 K) in the present study is again illustrated (blue). Tunneling through or passage over TS<sub>syn</sub> yields the initial HPB-2 energy distribution (red), which is obtained by scaling the *syn*-MECI thermal distribution by its tunneling-weighted unimolecular decay rates k(E) computed using statistical RRKM theory.<sup>22,47</sup> In this case, the initial HPB-2 distribution is peaked at higher energy, ca. 14.0 kcal mol<sup>-1</sup> above the OH + 2-butanone-3-yl product asymptote, suggesting a considerably greater OH + 2-butanone-3-yl product yield under the present experimental conditions. Under atmospheric conditions, some HPB-2 may be collisionally stabilized (blue), albeit in a ca. 3.0 kcal mol<sup>-1</sup> shallower well than HPB-1, and/or undergo subsequent decay from a thermal distribution shown at the O'-O elongation TS (red).

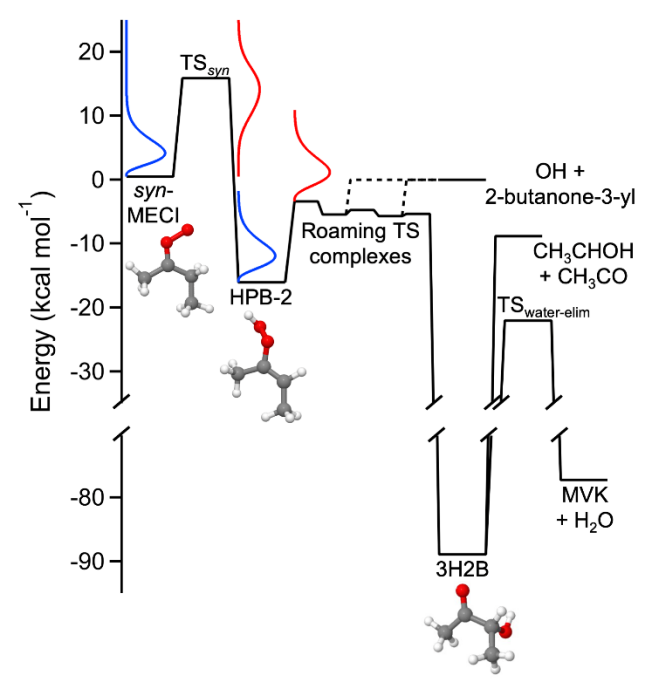


Figure 7. Reaction coordinate for the unimolecular pathways leading from the *syn*-conformer of MECI with energies relative to the OH + 2-butanone-3-yl product asymptote. Unimolecular decay proceeds via TS<sub>syn</sub> to 2-hydroperoxy-but-2-ene (HPB-2), followed by roaming of the separating OH and 2-butanone-3-yl radicals via roaming TS and complexes. This decay leads to OH + 2-butanone-3-yl radicals, 3-hydroxy-2-butanone (3H2B), hydroxyethyl (CH<sub>3</sub>CHOH) + acetyl (CH<sub>3</sub>CO) radicals, and/or methyl vinyl ketone (MVK) + H<sub>2</sub>O products via deeply submerged barrier TS<sub>water-elim</sub>. Boltzmann distributions (298 K) for *syn*-MECI (blue), HPB-2 (blue), and the first roaming TS (red) are illustrated. The initial HPB-2 distribution (red) is derived from the *syn*-MECI thermal distribution based on its energy-dependent unimolecular decay rates with tunneling.

# 2. Minimum Energy Pathways for Roaming

The theoretical analysis initially focuses on the minimum energy pathway (MEP) for the roaming mechanism from HPB-1 to 1H2B, shown in Figure 8, and then briefly describes the equivalent pathway available from HPB-2 to 3H2B (Figure 9). This discussion is followed by mapping of roaming-induced abstraction pathways from 1H2B and 3H2B leading to additional products (Figures 10-12). In each case, we have selected two coordinates, distance R and angle  $\theta$  that reflect the position and angular orientation of the roaming radical in the addition or abstraction process. Prior theoretical studies of the unimolecular decay of syn-CH<sub>3</sub>CHOO, (CH<sub>3</sub>)<sub>2</sub>COO, and MVK-oxide have also predicted roaming pathways. <sup>10-11</sup>

As shown in Figure 8 and video in Supporting Information, the roaming pathway of HPB-1 (the 1,4 hydrogen transfer product from the C1 carbon of *anti*-MECI) starts with O'-O bond elongation, where O' is the central oxygen of the OOH group on C2. The direction of the elongation increases the C1-O distance (displayed along the abscissa of Figure 8) while passing over a submerged barrier (TS-1a) and leads to an intermediate well of reaction complex RC-1a. In RC-1a the hydrogen of OH orients towards

the oxygen of the carbonyl group of 2-butanone-1-yl for a weakly stabilizing interaction in the long-range region of the potential. As such, the RC-1a configuration is 4.4 kcal mol<sup>-1</sup> lower than the dissociated OH and 2-butanone-1-yl radicals when using our best multireference based estimate (including the zero-point energy), as described in Sec. ST. While maintaining the hydrogen-carbonyl interaction, the OH radical will roam from the C1-distant side of 2-butanone-1-yl (in RC-1a) to the C1 side (in RC-1b) in a relatively flat region of the potential via a submerged barrier TS-1b (evident by the sign and magnitude of the  $\theta_{\rm OC2O}$  angle in Figure 8). Notably, the OH group is then near the unsaturated C1H<sub>2</sub> group of 2-butanone-1-yl (RC-1b). Roaming-induced isomerization can then occur by addition of the OH fragment to the C1 methylene group of 2-butanone-1-yl via submerged barrier TS-1c to yield 1H2B products. Under thermalized conditions, the roaming path will generally lead to collisional stabilization of 1H2B products in its deep well (-89.4 kcal mol<sup>-1</sup>). As a result, the roaming pathway could potentially reduce the OH yield in unimolecular decay of MECI.

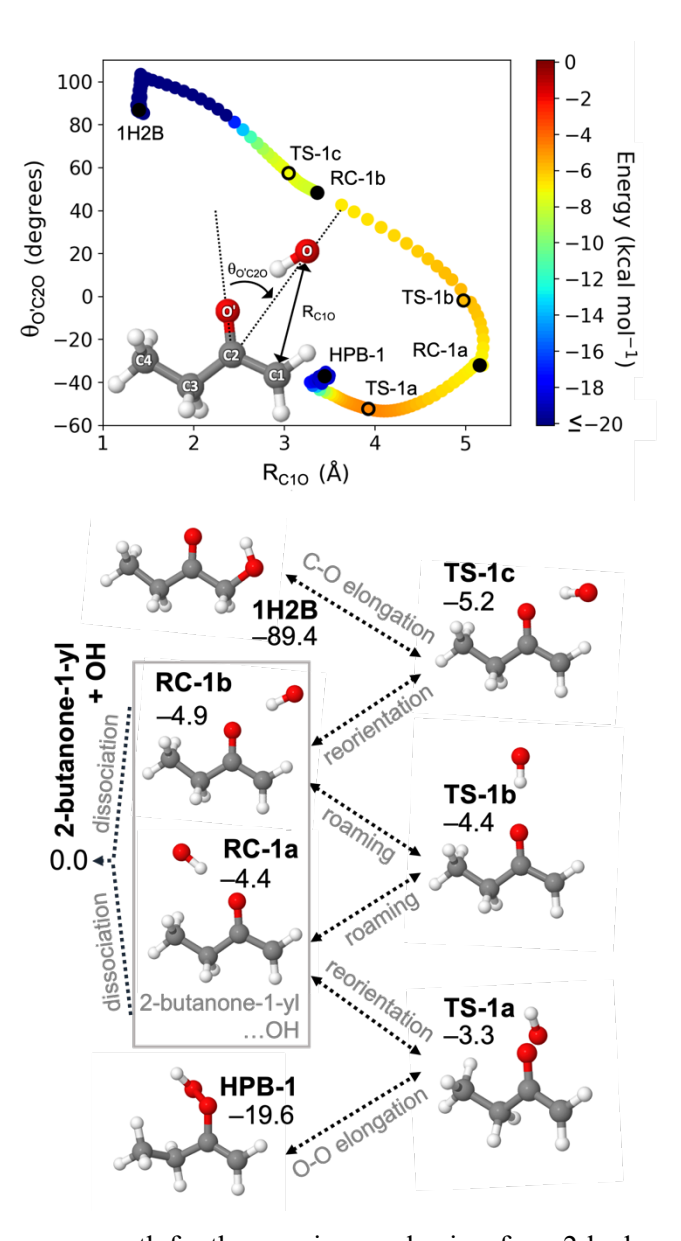


Figure 8. (Top) Minimum energy path for the roaming mechanism from 2-hydroperoxy-but-1-ene (HPB-1) to 1-hydroxy-2-butanone (1H2B) is displayed as a function of two coordinates, C1O bond distance (R<sub>C1O</sub>) and O'C2O angle ( $\theta_{\rm O'C2O}$ ), as shown in the inset structure. We define negative values for this angle as ones for which the magnitude of the OO'C2C1 torsional angle is greater than 90 degrees. The color gradient represents the CASPT2/cc-pVTZ calculated electronic energy (kcal mol<sup>-1</sup>) relative to separated 2-butanone-1-yl + OH products. Labeled points include roaming complexes in solid circles (RC-1a and RC-1b) and submerged transition states in open circles (TS-1a, TS-1b, TS-1c) along the pathway. The minimum energy pathway is also shown in a supplementary video. (Bottom) Molecular configurations at the labeled points starting with O'-O bond elongation of HPB-1, reorientation and roaming of 2-butanone-1-yl + OH fragments, and C-O bond formation leading to 1H2B products. Energies displayed beside each structure are the present best estimates of the zero-point corrected energies in kcal mol<sup>-1</sup> relative to 2-butanone-1-yl + OH products.

The roaming pathway of HPB-2 (the 1,4 hydrogen transfer product from the C3 carbon of *syn*-MECI) to 3H2B products shown in Figure 9 and videos in Supporting Information is similar to that for HPB-1 to

1H2B (Figure 8). Again, rather than fully dissociate, however, the OH may roam in a flat region that is 5-6 kcal mol<sup>-1</sup> lower in energy than the separated OH and 2-butanone-3-yl products. Ultimately, the oxygen of OH, labeled O in Figure 9, aligns with and adds to the unsaturated C3 of 2-butanone-3-yl to form a deep well (-88.9 kcal mol<sup>-1</sup>) of 3H2B, and the individual steps are not repeated here. The proximity of the CH group in 2-butanone-3-yl to the terminal methyl group presents an additional pathway that is not available to 1H2B. We focus on the subsequent C3-O bond extension of 3H2B, releasing the OH group that then roams in the vicinity of the C4 methyl group of 2-butanone-3-yl. Figure 9 displays the increase in the C3-O distance, R<sub>C3O</sub>. This leads to roaming-induced H-atom abstraction and transfer to OH, yielding MVK +  $H_2O$  products in another deep well (-77.2 kcal mol<sup>-1</sup>). Notably, the TS barrier (TS-2d) leading to MVK + H<sub>2</sub>O lies higher in energy than that associated with roaming to 3H2B (TS-2a), but both are submerged relative to the 2-butanone-3-yl + OH product asymptote. We find no minimum energy pathway from either RC-2a or RC-2b in which OH can directly roam to C4 to abstract a hydrogen to produce MVK + H<sub>2</sub>O that does not also require O to align towards C3. The O and C3 interaction, in each case, results in the formation of 3H2B. Note that alternative pathways would be possible if RC-2a or RC-2b were in a trans configuration, but the torsion to transition out of the cis configuration, shown in Figure 9, is rigid because the C2-C3 bond is resonant with the carbonyl. While the depth of the 3H2B well is likely to prevent a significant production of MVK + H<sub>2</sub>O via TS-2d, both the 3H2B and MVK + H<sub>2</sub>O producing pathways could potentially reduce the alternative 2-butanone-3-yl and OH yield. Sec. ST2 discusses branching ratios of these competing pathways.

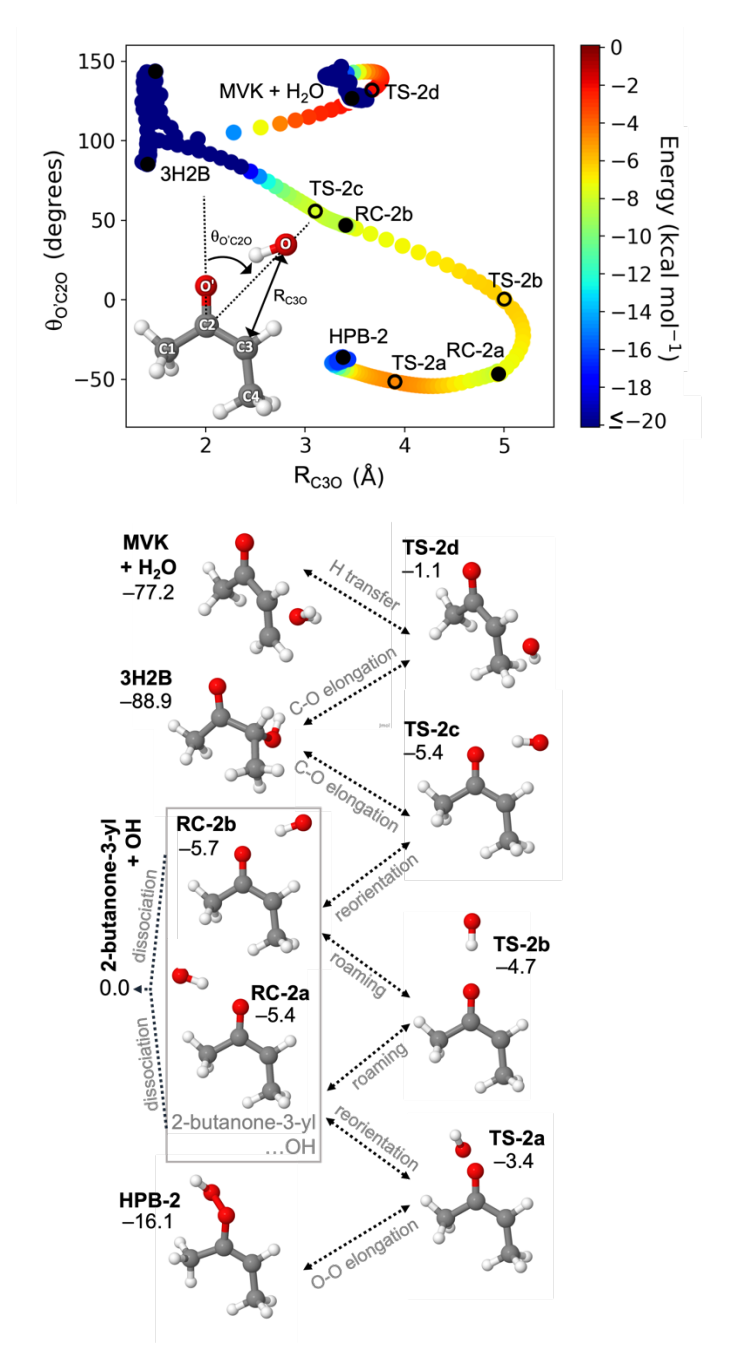


Figure 9. (Top) Minimum energy path for the roaming mechanism from 2-hydroperoxy-but-2-ene (HPB-2) to 3-hydroxy-2-butanone (3H2B) and MVK +  $H_2O$  products is displayed as a function of two coordinates, C3O bond distance ( $R_{C3O}$ ) and O'C2O angle ( $\theta_{O'C2O}$ ), as shown in the inset structure. We define negative values for this angle as ones for which the magnitude of the OO'C2C1 torsional angle is greater than 90 degrees. The color gradient represents the CASPT2/cc-pVTZ calculated electronic energy (kcal mol<sup>-1</sup>) relative to separated 2-butanone-3-yl + OH products. Labeled points include roaming complexes in solid circles (RC-2a and RC-2b) and submerged transition states in open circles (TS-2a, TS-2b, TS-2c, TS-2d) along the pathway. The minimum energy pathway is also shown in a supplementary video. (Bottom) Molecular configurations at the labeled points starting with O'-O bond elongation of HPB-2, roaming of 2-butanone-3-yl + OH fragments, and C3-O bond formation leading to 3H2B products. Subsequent C-O elongation, roaming of OH in the vicinity of the CH<sub>3</sub> group of 2-butanone-3-yl, and H-atom abstraction yields MVK +  $H_2O$  products. Energies displayed beside each structure are the

present best estimates of the zero-point-corrected energy in kcal mol<sup>-1</sup> relative to separated 2-butanone-3-yl + OH products (in the *cis* configuration).

As shown in Figure 10, alternative C1–C2 bond elongation of 1H2B can lead to roaming of the hydroxy methyl (CH<sub>2</sub>OH) radical in the vicinity of the propionyl (CH<sub>3</sub>CH<sub>2</sub>CO) radical at energies below the 2-butanone-1-yl + OH asymptote. For that plot, energies are relative to the separated hydroxy methyl and propionyl radicals, which lies 8.5 kcal mol<sup>-1</sup> below the 2-butanone-1-yl + OH product asymptote. During the initial C1–C2 bond elongation from 1H2B, the CH<sub>2</sub>OH radical reorients through TS-3a to reaction complex RC-3a so that the hydrogen of OH has a long-range interaction with the carbonyl of propionyl. The CH<sub>2</sub>OH radical subsequently roams, in order, through TS-3d, RC-3c, TS-3e, RC-3d, TS-3f, and RC-3e, while preserving the OH..O' interaction, and ultimately abstracts H3 (TS-3g) from the secondary C3 of the propionyl radical with its unsaturated C1, forming methanol (CH<sub>3</sub>OH) + methyl ketene (MK, CH<sub>3</sub>CHCO). Alternatively, the CH<sub>2</sub>OH radical can roam in such a way that the hydrogen of OH interacts with carbonyl C2 of the propionyl radical as it goes through TS-3b to RC-3b. This reaction complex allows for a roaming-induced H-atom transfer from the OH of CH<sub>2</sub>OH (TS-3c) to the C2 of the propionyl radical, forming products formaldehyde (H<sub>2</sub>CO) + propionaldehyde (PPA, CH<sub>3</sub>CH<sub>2</sub>CHO).

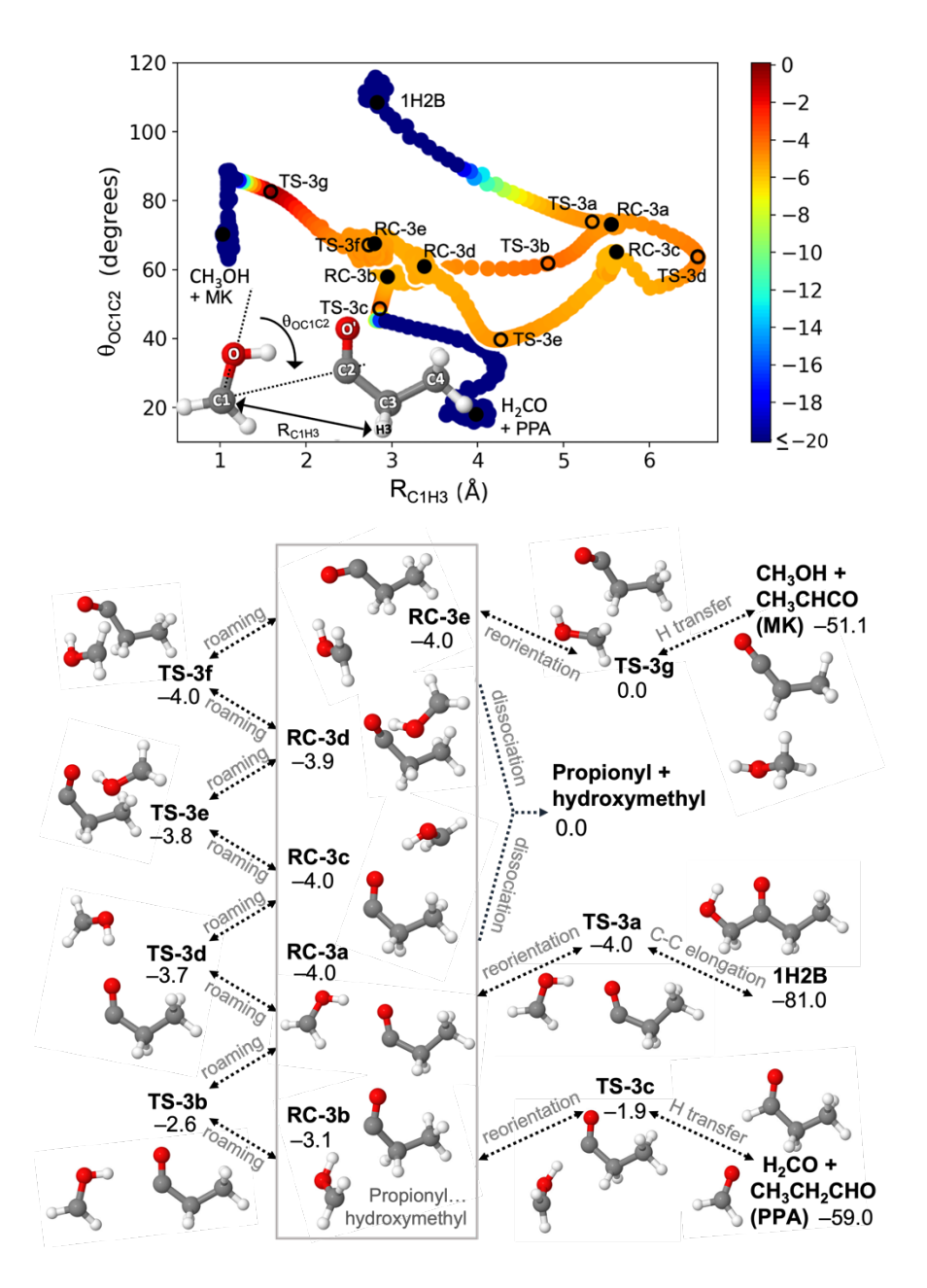


Figure 10. (Top) Minimum energy path for the roaming mechanism from 1-hydroxy-2-butanone (1H2B) to methanol (CH<sub>3</sub>OH) + methyl ketene (MK, CH<sub>3</sub>CHCO) and formaldehyde (H<sub>2</sub>CO) + propionaldehyde (PPA, CH<sub>3</sub>CH<sub>2</sub>CHO). Roaming pathways are displayed as a function of two coordinates, C1H3 bond distance (R<sub>C1H3</sub>) and OC1C2 angle ( $\theta_{OC1C2}$ ) as shown in inset structure. The color gradient represents the CASPT2/cc-pVTZ calculated electronic energy (kcal mol<sup>-1</sup>) relative to the separated hydroxy methyl and propionyl radicals. Labeled points include many roaming complexes in solid circles (RC-3) and transition states in open circles (TS-3) along two pathways. (Bottom) Molecular configurations at the labeled points start with C1–C2 elongation of 1H2B, roaming of the hydroxymethyl radical (CH<sub>2</sub>OH) relative to the propionyl radical (CH<sub>3</sub>CH<sub>2</sub>CO), and H-transfer from O to C2 forming H<sub>2</sub>CO + PPA. Molecular configurations also illustrate roaming of the hydroxymethyl radical (CH<sub>2</sub>OH) relative to the propionyl radical (CH<sub>3</sub>CH<sub>2</sub>CO) with H3-transfer from C3 to C1, forming methanol (CH<sub>3</sub>OH) + methyl ketone (MK, CH<sub>3</sub>CHCO). Energies displayed beside each structure are best estimates of the zero-point-

corrected energies relative to the separated hydroxy methyl and propionyl radicals, which in turn lies 8.5 kcal mol<sup>-1</sup> below the OH + 2-butanone-1-yl product asymptote.

The roaming pathways for trans- and cis-3H2B are shown in Figure 11 and Figure 12, respectively. While the torsional barrier between the two conformers is insignificant, the two conformers do provide distinct pathways and the two surfaces are separated for visual simplicity. Upon C2-C3 bond elongation in cis/trans-3H2B, 1-hydroxyethyl radical (CH3CHOH) roams relative to the acetyl radical (CH3CO), (where the separated radicals are 9.3 kcal mol<sup>-1</sup> below the syn-MECI reactant energy and 8.9 kcal mol<sup>-1</sup> below the separated OH and cis-2-butanone-3-yl radicals) before reorienting for a hydrogen transfer. All relative energies in Figures 11 and 12 correspond to the lowest energy conformation of the fully separated radical products. For trans-3H2B, the C2-C3 elongation is via TS-4a, which leads to a reaction complex, RC-4a, in which the hydrogen of the OH orients for a long-range interaction with the carbon of the acetyl radical carbonyl, C2. This hydrogen subsequently transfers to C2 via TS-4g to produce two acetaldehydes (AC, CH<sub>3</sub>CHO). Alternatively, 1-hydroxyethyl radical may roam through TS-4b so that its terminal methyl group interacts with the O' in the acetyl radical. The flat region of the potential extends via a pathway from RC-4b to RC-4c through TS-4c, where the 1-hydroxyethyl radical roams towards an interaction between the methyl of 1-hydroxyethyl and C2. The hydrogen of the methyl group in 1hydroxyethyl radical is labeled H in Figure 11, and the roaming from RC-4a to RC-4c is visible from the lessening of the C2H4 bond distance (R<sub>C2H4</sub>). The alignment in RC-4c enables a roaming-induced hydrogen transfer of H4 to C2 with an extremely low barrier via TS-4e to form AC and vinyl alcohol (VA, CH<sub>2</sub>CHOH). Additionally, the 1-hydroxyethyl radical may roam in a different direction starting from RC-4a through TS-4d so that the hydrogen on the terminal methyl, C1, of acetyl radical interacts with the radical carbon, C3, of the 1-hydroxyethyl radical, which forms RC-4d. This roaming is evident in Figure 11 by the change in the C3C2C1 bond angle ( $\theta_{C3C2C1}$ ) in these reaction complexes. Roaminginduced hydrogen transfer of the C1 hydrogen to C3 produces ethanol (ET, CH<sub>3</sub>CH<sub>2</sub>OH) and ketene (KE, CH<sub>2</sub>CO) after proceeding over a small barrier in TS-4f.

The roaming-induced hydrogen transfers for *cis*-3H2B lead to the same products as for the *trans*-configuration, but the initial C2–C3 bond elongation first forms a reaction complex RC-4h in which the hydrogen of the OH interacts with O'. Because of this, the 1-hydroxyethyl must step through an additional roaming pathway (TS-4i, RC-4i, TS-4l) before forming 2AC with a barrier to the hydrogen transfer that is 1.2 kcal mol<sup>-1</sup> lower than for the *trans*-surface (TS-4g). In contrast, the ET + KE barrier is 1.0 kcal mol<sup>-1</sup> higher for the *cis*-surface (TS-4m and TS-4f) and the AC + VA barrier is similar in energy (TS-4n and TS-4e) despite involving an interaction between the hydrogen of OH with O'.

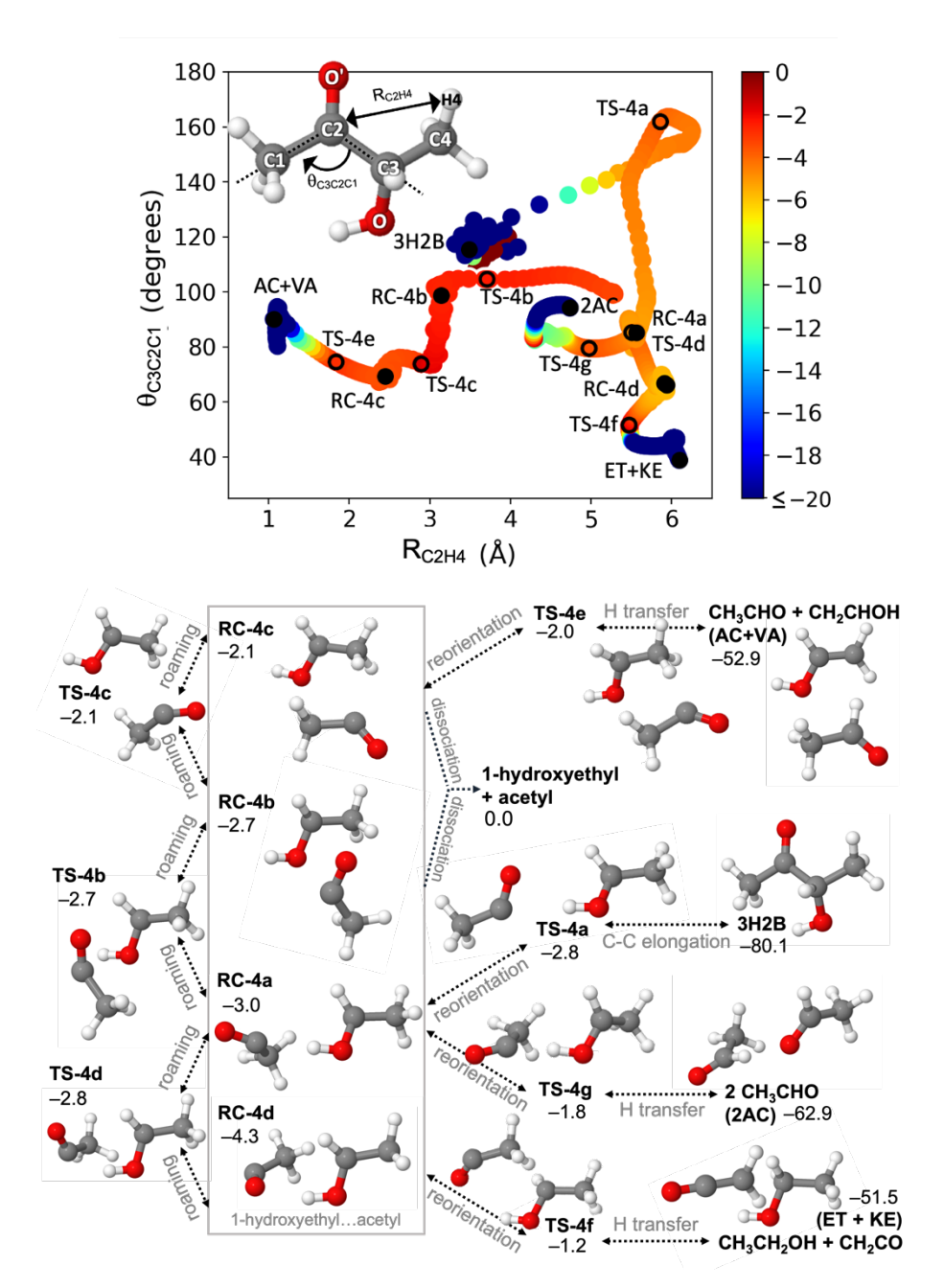


Figure 11. (Top) Minimum energy path for the roaming mechanism from *trans*-3-hydroxy-2-butanone (*trans*-3H2B) to acetaldehyde (AC, CH<sub>3</sub>CHO) + vinyl alcohol (VA, CH<sub>2</sub>CHOH), 2AC, and ethanol (ET, CH<sub>3</sub>CH<sub>2</sub>OH) + ketene (KE, CH<sub>2</sub>CO). Roaming pathways are displayed as a function of two coordinates, C2H4 bond distance ( $R_{C2H4}$ ) and C3C2C1 angle ( $\theta_{C3C2C1}$ ) shown in inset structure. The color gradient represents the CASPT2/cc-pVTZ calculated electronic energy (kcal mol<sup>-1</sup>) relative to separated 2-butanone-3-yl + OH products. Labeled points include many roaming complexes in solid circles (RC-4) and transition states in open circles (TS-4) along two pathways. (Bottom) Molecular configurations at the labeled points start with C2–C3 elongation of *trans*-3H2B, roaming of the 1-hydroxyethyl radical (CH<sub>3</sub>CHOH) relative to the acetyl radical (CH<sub>3</sub>CO), and H-transfer from O to C2 forming 2AC. Molecular configurations also illustrate roaming of the acetyl radical (CH<sub>3</sub>CO) relative to the 1-hydroxyethyl radical (CH<sub>3</sub>CHOH) with H-transfer from C4 to C2, forming AC + VA, and from C1 to C3 to form ET + KE. Energies displayed beside each structure are the best estimates of the zero-point-

corrected energy in kcal mol<sup>-1</sup> relative to separated 1-hydroxyethyl + acetyl products, which in turn lies 8.9 kcal mol<sup>-1</sup> below the OH + cis-2-butanone-3-yl product asymptote.

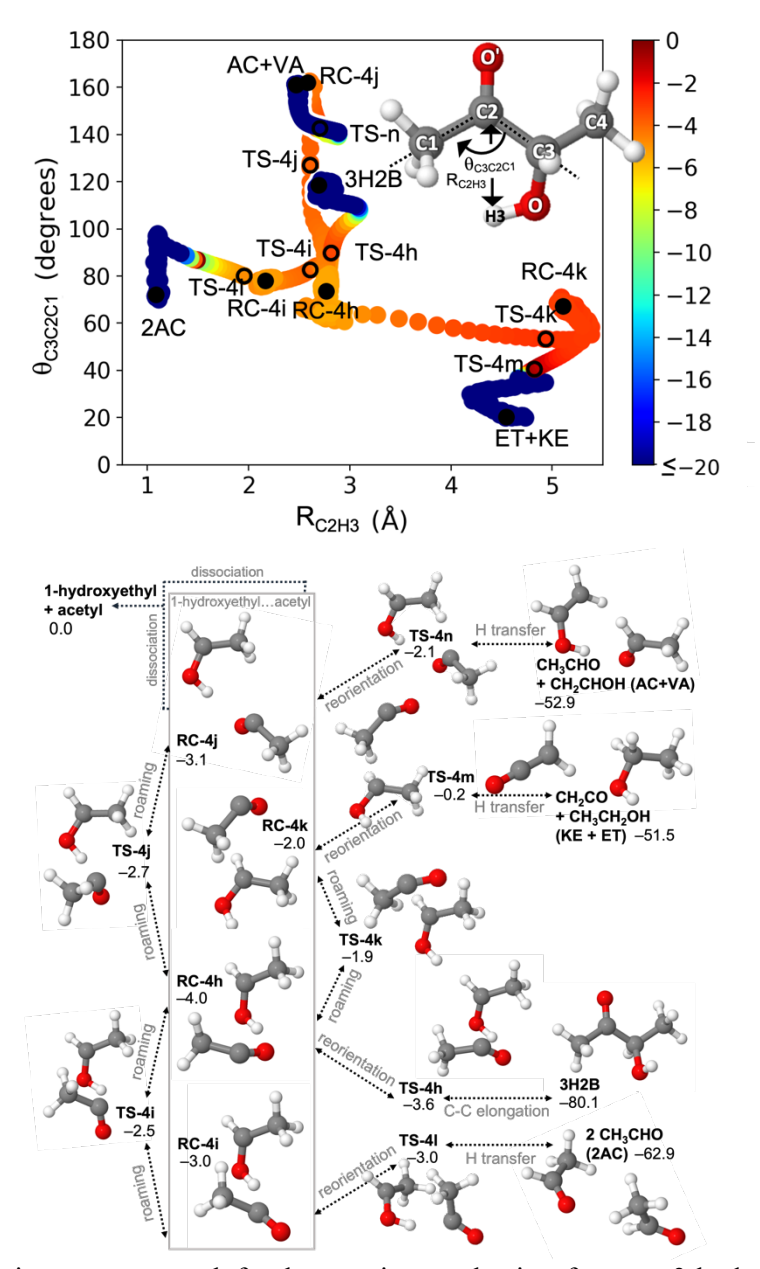


Figure 12. (Top) Minimum energy path for the roaming mechanism from cis-3-hydroxy-2-butanone (cis-3H2B) to acetaldehyde (AC, CH<sub>3</sub>CHO) + vinyl alcohol (VA, CH<sub>2</sub>CHOH), 2AC, and ethanol (ET, CH<sub>3</sub>CH<sub>2</sub>OH) + ketene (KE, CH<sub>2</sub>CO). Roaming pathways are displayed as a function of two coordinates, C2H3 bond distance ( $R_{C2H3}$ ) and C3C2C1 angle ( $\theta_{C3C2C1}$ ). The color gradient represents the CASPT2/cc-pVTZ calculated electronic energy (kcal mol<sup>-1</sup>) relative to separated 2-butanone-3-yl + OH products. Labeled points include many roaming complexes in solid circles (RC-4) and transition states in open circles (TS-4) along two pathways. (Bottom) Molecular configurations at the labeled points start with C2–C3 elongation of cis-3H2B, roaming of the 1-hydroxyethyl radical (CH<sub>3</sub>CHOH) relative to the acetyl radical (CH<sub>3</sub>CO), and H-transfer from O to C2 forming 2AC. Molecular configurations also illustrate roaming of the acetyl radical (CH<sub>3</sub>CO) relative to the 1-hydroxyethyl radical (CH<sub>3</sub>CHOH) with H-transfer from C4 to C2, forming AC + VA, and from C1 to C3 to form ET + KE. Energies displayed beside each

structure are the best estimates of the zero-point-corrected energy in kcal  $mol^{-1}$  relative to separated 1-hydroxyethyl + acetyl products, which in turn lies 8.9 kcal  $mol^{-1}$  below the OH + cis-2-butanone-3-yl product asymptote.

#### E. Discussion

The experimental and theoretical studies of MECI at low pressure (10 Torr or 0.01 bar), thermal conditions (298 K) show a significant propensity for unimolecular decay via roaming pathway(s) in addition to conventional O-O bond fission to OH + butanonyl radicals. Unimolecular decay of *anti-* and *syn-*conformers of MECI proceeds by H-atom transfer from a methyl (*anti*) or methylene (*syn*) group to the terminal oxygen, forming hydroperoxybutene (HPB-1 or HPB-2) intermediates, which is followed by O-O bond elongation, leading to conventional O-O fission, or alternatively to many theoretically predicted roaming pathways (Figures 8-12). The present experiments conducted under thermal flow cell conditions identify stable products resulting from roaming, specifically hydroxybutanone (1H2B and/or 3H2B, Figures 2-3) and methyl vinyl ketone (MVK, Figure 5), by their distinctive photoionization spectra, kinetic temporal profiles, and mass. As discussed in Sec. C4 (and Sec. SE3), we estimate a lower limit for the 1H2B yield of ca. 7% resulting from unimolecular decay of MECI under the laboratory flow cell conditions (10 Torr, 298 K).

A comprehensive theoretical kinetic analysis of the rate constants and branching to products that arise from unimolecular decay of *anti-* and *syn-*MECI is presented in Sec. ST. In brief, the kinetic analysis involves a combination of variable reaction coordinate (VRC) - transition state theory (TST) analyses<sup>48-49</sup> for the key radical-radical channels together with conventional TST analyses<sup>50</sup> for the remaining channels. Master equation simulations<sup>51-52</sup> incorporating these TST analyses provide predictions for the rate constants and branching for the overall kinetic process starting from MECI. This kinetic analysis builds from a statistical theory for roaming presented earlier.<sup>12</sup> Here, we focus on the predicted temperature and pressure dependencies of the branching fraction for conventional O-O dissociation and roaming processes resulting from thermal unimolecular decay of *anti-*conformers of MECI. Analogous results for *syn-*conformers of MECI show significantly less branching to roaming as detailed in Sec. ST2.

The predicted branching ratios for the three primary product channels in the thermal unimolecular decay of *anti*-MECI are shown in Figure 13 as a function of temperature from 200 to 350 K for pressures of 0.01 and 1 bar N<sub>2</sub>, which are representative of experimental flow cell and atmospheric conditions, respectively (see also Figures ST3 and ST5). Three different models for roaming are utilized: a reference model (solid line) where the electronic states are treated statistically; a slow electronic state conversion or single state (SS) model (dotted line) with only the ground electronic state accessible; and a rapid roaming (RR) model (dashed line) using a statistical treatment of electronic states with a rapid roaming process (see ST for further details). The product branching upon thermal unimolecular decay of *anti*-MECI at

0.01 bar (top panel) is effectively temperature-independent from 200 to 350 K with conventional O-O dissociation to OH + 2-butanone-1-yl (black) of 89-90% (reference model), which decreases to 74-77% for the SS and RR models. The primary product of roaming, 1-hydroxy-2-butanone (1H2B, blue), accounts for 10-11% yield (reference model), in good accord with the estimated experimental yield of ca. 7% as shown in Figure 13, and increases to 23-26% yield for SS and RR models. The 2-hydroperoxy-but-1-ene (HPB-1) intermediate is not predicted to be stabilized at low pressure (0.01 bar N<sub>2</sub>).

At atmospheric pressure (1 bar, bottom panel), the OH + 2-butanone-1-yl product (black) from conventional O-O dissociation has a lower yield and exhibits a temperature dependence between 200 and 350 K, increasing from 73% at 200 K to 86% at 350 K (reference model). The conventional product yield decreases to 58-74% for the SS and RR models. By contrast, the branching fraction to the 1H2B roaming product (blue) is similar from 200 to 350 K at 1 bar and lower pressure with 10-13% yield. The SS and RR models predict a 2-fold greater 1H2B yield. There is a notable increase in stabilization of HPB-1 (teal) at 1 bar ranging from 5 to 15% with decreasing temperature (similar for the 3 models), particularly at  $T \le 300$  K. The increased stabilization of HPB-1 at 1 bar correlates with a decrease in the OH + 2-butanone-1-yl yield at atmospheric conditions.

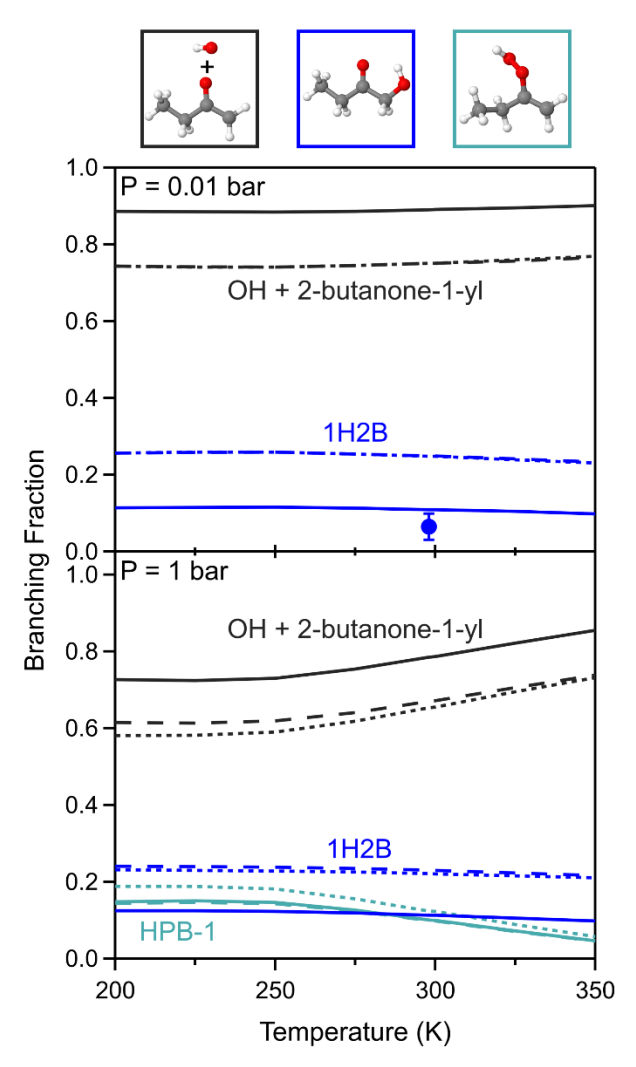


Figure 13. Temperature dependence of the predicted product branching fractions for the unimolecular decay of *anti*-MECI to OH + 2-butanone-1-yl (black), 1-hydroxy-2-butanone (1H2B, blue), and 2-hydroperoxy-but-1-ene (HPB-1, teal) at a pressure of 0.01 bar (top), analogous to flow cell conditions, and 1 bar (bottom) of relevance to the troposphere. The predictions for the single state (SS, dotted) and rapid roaming (RR, dashed) cases are coincidentally overlapping (top) or nearly overlapping (bottom). Also shown is the estimated experimental lower limit for the 1H2B yield of ca. 7% resulting from unimolecular decay of MECI under the laboratory flow cell conditions. This figure is replotted as Figure ST3 and ST5 in the SI.

The theoretical kinetic analysis also provides insights on the pressure-dependence of branching to conventional and roaming products that result from unimolecular decay of *anti*-MECI at 298 K as shown in Figure 14 (see also Figure ST7). The yield of conventional OH + 2-butanone-1-yl products is essentially unchanged at 88% for pressures from 0.001 to 0.1 bar and falls off to 79% (reference model) at atmospheric pressure (1 bar). The RR and SS models predict a consistent 15% lower yield over the 0.001 to 1 bar range. The yield of the primary roaming product, 1H2B, is approximately constant at 10-11% from 0.001 to 1 bar; the RR and SS models predict a two-fold greater 1H2B yield. Finally, the 2-

hydroperoxy-but-1-ene (HPB-1, teal) intermediate is collisionally stabilized at pressures from ca. 0.3 to 1 bar with yield of 2 to 10%, which primarily reduces the OH + 2-butanone-1-yl yield. At 1 bar, the yield of HPB-1 is similar to that of 1H2B.

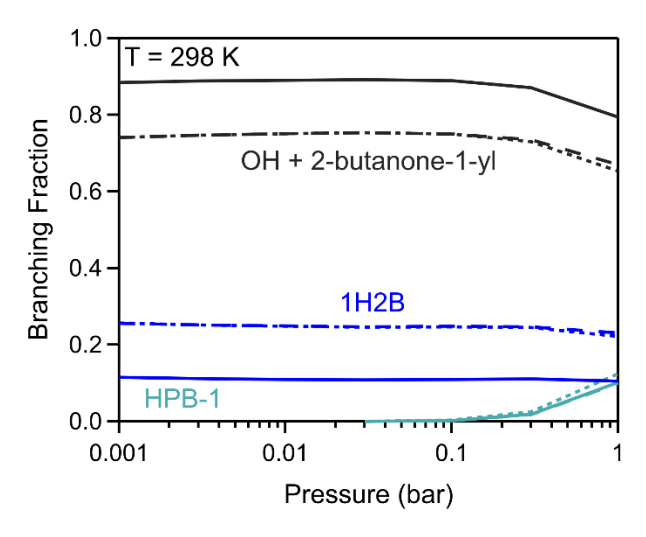


Figure 14. Pressure-dependence of the predicted product branching fractions to OH + 2-butanone-1-yl (black), 1-hydroxy-2-butanone (1H2B, blue), and 2-hydroperoxy-but-1-ene (HPB-1, teal) for the unimolecular decay of *anti*-MECI at 298 K. A pressure of 0.01 bar is analogous to the current experimental flow cell conditions, while 1 bar is of relevance to the troposphere. The predictions for the single state (SS, dotted) and rapid roaming (RR, dashed) cases are coincidentally overlapping or nearly overlapping. This figure is replotted as Figure ST7 in the SI.

An analogous theoretical kinetic analysis of the roaming products from *syn*-MECI (see ST) reveals a smaller branching fraction to 3-hydroxy-2-butanone (3H2B) of ca. 5% at both 0.01 and 1 bar pressure (Figures ST4 and ST6), compared to ca. 10-12% yield for 1H2B roaming products from *anti*-MECI at 0.01 and 1 bar, in both cases at temperatures from 200-350 K. This suggests that the experimentally observed hydroxybutanone (Figures 2 and 3) arises primarily from unimolecular decay of *anti*-MECI. In addition, there is negligible stabilization of the 2-hydroperoxy-but-2-ene (HPB-2) intermediate derived from *syn*-MECI (Figure ST6) compared to the 10% yield for HPB-1 from *anti*-MECI at 1 bar, 298 K, reflecting both the hotter initial distribution and shallower well of the HPB-2 intermediate (Figures 6 and 7).

The smaller roaming component upon unimolecular decay of *syn*-MECI compared to that for *anti*-MECI can be rationalized based on the relative energies of the Criegee intermediates compared to their OH + butanonyl product asymptotes (Figures 6 and 7). For *syn*-MECI, the reactant lies 0.5 kcal mol<sup>-1</sup> *above* the product asymptote, facilitating conventional O-O bond breaking and reducing the likelihood of roaming to 3H2B. For *anti*-MECI, the reactant lies 3.9 kcal mol<sup>-1</sup> *below* the product asymptote, thereby reducing the probability of dissociation and increasing the likelihood of roaming to 1H2B. The relative energies of the 2-butanone-1-yl and 2-butanone-3-yl radical products can be rationalized based on the

delocalized nature of the radical involving a primary vs. more stable secondary carbon site and the oxygen, respectively.<sup>22</sup>

The stabilization of vinyl hydroperoxide, HPB-1, particularly at low temperatures (T < 300 K) and atmospheric pressure (Figures 13-14; ST5, ST7), is reminiscent of an earlier theoretical study by Kuwata et al. on the unimolecular decay of the acetone oxide (CH<sub>3</sub>)<sub>2</sub>COO<sup>10</sup> and even earlier work by Donahue and coworkers. The Kuwata et al. study predicted that low temperatures (200 K) and high pressures (1 atm) favored the temporary accumulation of the vinyl hydroperoxide intermediate derived from thermalized (CH<sub>3</sub>)<sub>2</sub>COO prior to rearranging to hydroxyacetone products, associated with OH roaming, or decomposing to OH + 1-methyl vinoxy radicals. Hydroxyacteone has also been directly observed upon unimolecular decay of (CH<sub>3</sub>)<sub>2</sub>COO in a prior study utilizing the MPIMS experimental approach. However, a parallel statistical rate study on *syn*-CH<sub>3</sub>CHOO predicted little accumulation of vinyl hydroperoxide or hydroxyacetaldehyde products under analogous thermal conditions.

Finally, one can envision starting from fully stabilized HPB-1 and HPB-2 intermediates under atmospheric conditions (1 bar, 200-350 K), depicted by the Boltzmann distributions (blue) in Figures 6-7. In this case, the subsequent decay of HPB-1 or HPB-2 under thermal conditions (Figures 15 and ST9) follows primarily the lower energy pathway leading to hydroxybutanone products. The predicted yield is strongly temperature-dependent from 200 to 350 K with a decreasing yield of roaming products (1H2B and 3H2B by 30% and 10%, respectively) and a corresponding increase in the yield of conventional (OH + 2-butanonyl) products with increasing temperature. Modified Arrhenius fits of the theoretical predictions for the temperature and pressure dependent decay of *anti* and *syn*-MECI, HPB-1, and HPB-2 are provided in Sec. ST.

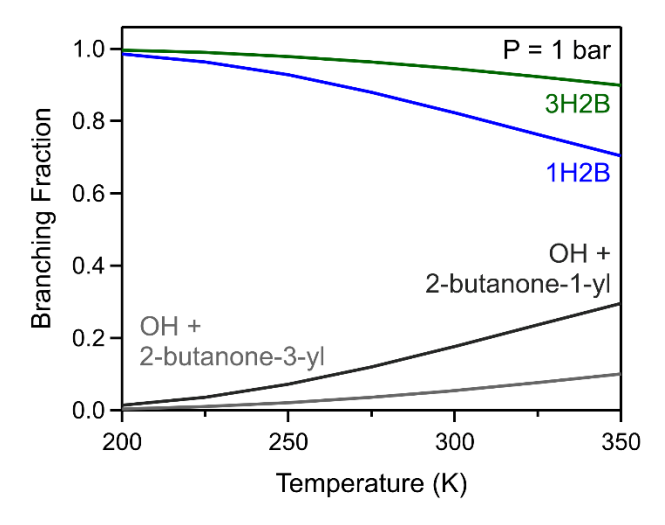


Figure 15. Temperature-dependence of the predicted product branching fractions for unimolecular decay of metastable HPB-1 to 1H2B (blue) and OH + 2-butanone-1-yl (black) and that for unimolecular decay

of metastable HPB-2 to 3H2B (green) and OH + 2-butanone-3-yl (gray) at a pressure of 1 bar. This figure is replotted as Figure ST9 in the SI.

Returning to the unimolecular decay of MECI under thermal conditions, the theoretical kinetic analysis also predicts branching to other products (Figures ST10 and ST11), primarily through C-O or C-C elongation of 1H2B and 3H2B. This can lead to numerous stable products through the roaming mechanisms detailed in Figures 9-12. The branching to MVK + H<sub>2</sub>O via C-O bond elongation of 3H2B and H-atom transfer (Figure 9) is of particular note since MVK is observed experimentally (Figure 5). This channel arises from *syn*-MECI primarily via a low-energy tight transition state (TS<sub>water-elim</sub>, Figure 7). An MVK yield of 0.2 to 0.6% relative to 3H2B is predicted with increasing temperatures (200 to 350 K, Figure ST11) at 0.01 bar, and is predicted to increase significantly at lower pressures (to 0.001 bar). The predicted MVK yield is notably lower than that estimated experimentally. Other stable products are anticipated (Figures ST10-ST11), but with low yields. C-C fragmentation of 1H2B and 3H2B may also occur, leading from 1H2B to hydroxy methyl (CH<sub>2</sub>OH) + propionyl (CH<sub>3</sub>CH<sub>2</sub>CO) radicals with small yield (< 0.1% relative to 1H2B) or from 3H2B to hydroxy ethyl (CH<sub>3</sub>CHOH) + acetyl (CH<sub>3</sub>CO) radicals with a few percent yield (relative to 3H2B). Any radicals formed, however, will rapidly react with O<sub>2</sub> in the flow tube. Under isolated jet-cooled conditions, however, we anticipate a more substantial yield of radical products through C-C fission of 1H2B and 3H2B.

## F. Conclusions

Hydroxybutanone (1H2B and/or 3H2B) has been identified as a stable product from unimolecular decay of the methyl-ethyl substituted Criegee intermediate (MECI) under thermal conditions in a flow tube coupled with multiplexed photoionization mass spectrometry detection. Hydroxybutanone, an isomer of MECI (m/z 88), arises from 1,4 H-atom transfer, followed by roaming and reorientation of the separating OH radical, leading to OH addition at the vinyl site of butanonyl. The hydroxybutanone product is identified by its photoionization spectrum, which has a distinctly higher threshold (9.5 eV) compared to that for MECI (8.7 eV). The photoionization spectrum of the hydroxybutanone product is consistent with the computed adiabatic ionization energies for 1H2B (9.2 eV) and 3H2B (9.4 eV) and that separately recorded for commercial samples of 1H2B (with absolute photoionization cross-section determination, Section SE3) and 3H2B. Moreover, the temporal appearance profile of hydroxybutanone leads to a persistent ionization signal at long time (ca. 40 ms), characteristic of a stable product, which mirrors the temporal decay profile associated with thermal unimolecular decay MECI. The origin of hydroxybutanone from the unimolecular decay of MECI is verified by scavenger experiments utilizing excess SO<sub>2</sub> to preferentially remove MECI via bimolecular reaction. An experimental branching yield to hydroxybutanone of ~7% is estimated under the experimental conditions of a slow-flow reactor (10 Torr,

298 K). A smaller yield of methyl vinyl ketone (MVK, m/z 70) is observed and ascribed to roaming, again based on its temporal appearance profile leading to a persistent photoionization signal at long time.

A complementary multi-reference electronic structure theoretical investigation has been undertaken to map the reaction coordinates associated with conventional and roaming pathways for unimolecular decay of *anti-* and *syn-*MECI. Unimolecular decay proceeds via 1,4 H-atom transfer from the methyl or methylene group to the terminal O-atom by surmounting or tunneling through a TS barrier, transiently forming a vinyl hydroperoxide (HPB-1 or HPB-2), followed by O-O elongation and reorientation and/or roaming of the radicals in the long-range region of the potential. The OH and butanonyl radicals can then separate or, alternatively, follow addition roaming pathways to yield hydroxybutanone (1H2B and/or 3H2B) products. Further C-O elongation of 3H2B and H-transfer can yield MVK + H<sub>2</sub>O products. Further C-C elongation of 1H2B or 3H2B, followed by reorientation, roaming, and H-transfer can result in many additional products.

A comprehensive variable reaction coordinate transition state theory based theoretical kinetic analysis has predicted rate constants and branching yields to products that arise from thermal unimolecular decay of *anti*- and *syn*-MECI by conventional and roaming pathways. The kinetic analysis is applied to pressure and temperature conditions similar to the present experiment (0.01 bar, 298 K) and extended to atmospheric conditions (1 bar, 200-350 K). The kinetic analysis shows that *anti*-MECI leads to the primary product of roaming, 1-hydroxy-2-butanone (1H2B), with a yield of 10-11% (based on a statistical treatment of electronic states) that is temperature independent from 200 to 350 K at 0.01 bar; other theoretical models for roaming (slow electronic state conversion or rapid roaming) increase the predicted 1H2B yield more than 2-fold. The predicted yield is in good accord with that estimated experimentally for hydroxybutanone of ca. 7%. The vinyl hydroperoxide (HPB-1) intermediate is not stabilized under thermal laboratory conditions. Under atmospheric conditions (1 bar, 200-350 K), both HPB-1 and 1H2B are stabilized, reducing the OH + 2-butanone-1-yl yield from *anti*-MECI. By contrast, thermal unimolecular decay of *syn*-MECI leads to a smaller branching fraction of roaming products under laboratory and atmospheric conditions. Other products of roaming, including MVK + H<sub>2</sub>O derived from *syn*-MECI, are predicted to have relatively low yields under laboratory and atmospheric conditions.

The combined experimental and theoretical study demonstrates and quantifies a significant yield for roaming to hydroxybutanone products in the unimolecular decay of MECI. Thus, formation of hydroxycarbonyl products is expected to be a general result of roaming in the thermal unimolecular decay of alkyl-substituted Criegee intermediates.<sup>9-11</sup> As a result, roaming can significantly reduce the yield of OH radicals produced from alkene ozonolysis via the 1,4 H-atom transfer mechanism under laboratory and atmospheric conditions.<sup>55</sup>

Associate Content

Data and materials availability

All data are available in the main text, supporting information, and Zenodo,<sup>56</sup> the latter of which contains the input file for the Master Equation System Solver (MESS).

Supporting Experimental (SE) Information includes additional photoionization results, estimated yields, and the fate of peroxy radicals. Supporting Theoretical (ST) Information contains details on the multireference electronic structure calculations, transition state theory analyses, and theoretical kinetic results of product branching with associated temperature and pressure dependencies. Supporting Information also contains videos illustrating the minimum energy pathways associated with roaming from HPB-1 or HPB-2 to hydroxybutanone (1H2B or 3H2B) products, which are also depicted in Figures 8 and 9.

### Acknowledgements

Research at the University of Pennsylvania is supported by the National Science Foundation under grants CHE-1955068 and CHE-2301298 with partial equipment support from the US Department of Energy-Basic Energy Sciences under grant DE-FG02-87ER13792. This work utilized the Extreme Science and Engineering Discovery Environment (XSEDE), which is supported by the National Science Foundation grant number ACI-1548562 through the allocation TG-CHE190088. C.A.S. acknowledges support from NSF CHE-2102626. Argonne National Laboratory is supported by the USDOE, Office of Science, BES, Division of Chemical Sciences, Geosciences, and Biosciences under Contract No. DE-AC02-06CH11357. Sandia National Laboratories is a multimission laboratory managed and operated by National Technology and Engineering Solutions of Sandia, LLC, a wholly owned subsidiary of Honeywell International, Inc., for the USDOE's National Nuclear Security Administration under contract DE-NA0003525. The operation of the multiplexed photoionization mass spectrometry kinetics experiments and the participation of the Sandia personnel was supported by Chemical Sciences, Geosciences, and Biosciences, Office of Basic Energy Sciences, of the U.S. Department of Energy. This research used resources of the Advanced Light Source, which is a DOE Office of Science User Facility under contract no. DE-AC02-05CH11231. This paper describes objective technical results and analysis. Any subjective views or opinions that might be expressed in the paper do not necessarily represent the views of the USDOE or the US Government. ©2022, California Institute of Technology. T.L. and M.I.L. thank Penn undergraduate Khaliun Dorjmenchim for making the videos. C.R.M. is grateful for support from an A. O. Beckman postdoctoral fellowship.

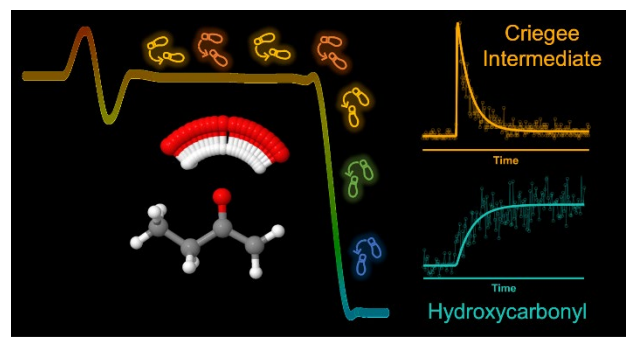
#### References

- 1. Johnson, D.; Marston, G., The gas-phase ozonolysis of unsaturated volatile organic compounds in the troposphere. *Chem. Soc. Rev.* **2008**, *37* (4), 699-716.
- 2. Sindelarova, K.; Granier, C.; Bouarar, I.; Guenther, A.; Tilmes, S.; Stavrakou, T.; Muller, J. F.; Kuhn, U.; Stefani, P.; Knorr, W., Global data set of biogenic VOC emissions calculated by the MEGAN model over the last 30 years. *Atmos. Chem. Phys.* **2014**, *14* (17), 9317-9341.
- 3. Osborn, D. L.; Taatjes, C. A., The physical chemistry of Criegee intermediates in the gas phase. *Int. Rev. Phys. Chem.* **2015**, *34* (3), 309-360.
- 4. Harrison, R. M.; Yin, J.; Tilling, R. M.; Cai, X.; Seakins, P. W.; Hopkins, J. R.; Lansley, D. L.; Lewis, A. C.; Hunter, M. C.; Heard, D. E.; Carpenter, L. J.; Creasy, D. J.; Lee, J. D.; Pilling, M. J.; Carslaw, N.; Emmerson, K. M.; Redington, A.; Derwent, R. G.; Ryall, D.; Mills, G.; Penkett, S. A., Measurement and modelling of air pollution and atmospheric chemistry in the UK West Midlands conurbation: Overview of the PUMA Consortium project. *Sci. Total Environ.* **2006**, *360* (1-3), 5-25.
- 5. Lester, M. I.; Klippenstein, S. J., Unimolecular Decay of Criegee Intermediates to OH Radical Products: Prompt and Thermal Decay Processes. *Acc. Chem. Res.* **2018**, *51* (4), 978-985.
- 6. Stephenson, T. A.; Lester, M. I., Unimolecular decay dynamics of Criegee intermediates: Energy-resolved rates, thermal rates, and their atmospheric impact. *Int. Rev. Phys. Chem.* **2020**, *39* (1), 1-33.
- 7. Chhantyal-Pun, R.; Khan, M. A. H.; Taatjes, C. A.; Percival, C. J.; Orr-Ewing, A. J.; Shallcross, D. E., Criegee intermediates: production, detection and reactivity. *Int. Rev. Phys. Chem.* **2020**, *39* (3), 385-424.
- 8. Caravan, R. L.; Vansco, M. F.; Lester, M. I., Open questions on the reactivity of Criegee intermediates. *Commun. Chem.* **2021**, *4* (1), 44.
- 9. Taatjes, C. A.; Liu, F.; Rotavera, B.; Kumar, M.; Caravan, R.; Osborn, D. L.; Thompson, W. H.; Lester, M. I., Hydroxyacetone Production From C3 Criegee Intermediates. *J. Phys. Chem. A* **2017**, *121* (1), 16-23.
- 10. Kuwata, K. T.; Luu, L.; Weberg, A. B.; Huang, K.; Parsons, A. J.; Peebles, L. A.; Rackstraw, N. B.; Kim, M. J., Quantum Chemical and Statistical Rate Theory Studies of the Vinyl Hydroperoxides Formed in trans-2-Butene and 2,3-Dimethyl-2-butene Ozonolysis. *J. Phys. Chem. A* **2018**, *122* (9), 2485-2502.
- 11. Barber, V. P.; Pandit, S.; Green, A. M.; Trongsiriwat, N.; Walsh, P. J.; Klippenstein, S. J.; Lester, M. I., Four-Carbon Criegee Intermediate from Isoprene Ozonolysis: Methyl Vinyl Ketone Oxide Synthesis, Infrared Spectrum, and OH Production. *J. Am. Chem. Soc.* **2018**, *140* (34), 10866-10880.
- 12. Klippenstein, S. J.; Georgievskii, Y.; Harding, L. B., Statistical Theory for the Kinetics and Dynamics of Roaming Reactions. *J. Phys. Chem. A* **2011**, *115* (50), 14370-14381.
- 13. Suits, A. G., Roaming Reactions and Dynamics in the van der Waals Region. *Annu. Rev. Phys. Chem.* **2020,** *71* (1), 77-100.
- 14. Kamarchik, E.; Koziol, L.; Reisler, H.; Bowman, J. M.; Krylov, A. I., Roaming Pathway Leading to Unexpected Water + Vinyl Products in C<sub>2</sub>H<sub>4</sub>OH Dissociation. *J. Phys. Chem. Lett.* **2010**, *1* (20), 3058-3065.
- 15. Niki, H.; Maker, P. D.; Savage, C. M.; Breitenbach, L. P.; Hurley, M. D., FTIR spectroscopic study of the mechanism for the gas-phase reaction between ozone and tetramethylethylene. *J. Phys. Chem.* **1987**, *91* (4), 941-946.
- 16. Grosjean, D.; Grosjean, E.; Williams, E. L., Atmospheric chemistry of olefins: a product study of the ozone-alkene reaction with cyclohexane added to scavenge hydroxyl radical. *Environ. Sci. Technol.* **1994,** *28* (1), 186-196.
- 17. Liu, F.; Beames, J. M.; Green, A. M.; Lester, M. I., UV Spectroscopic Characterization of Dimethyl- and Ethyl-Substituted Carbonyl Oxides. *J. Phys. Chem. A* **2014**, *118* (12), 2298-2306.
- 18. Kurten, T.; Donahue, N. M., MRCISD Studies of the Dissociation of Vinylhydroperoxide, CH<sub>2</sub>CHOOH: There Is a Saddle Point. *J. Phys. Chem. A* **2012**, *116* (25), 6823-6830.

- 19. Kidwell, N. M.; Li, H. W.; Wang, X. H.; Bowman, J. M.; Lester, M. I., Unimolecular dissociation dynamics of vibrationally activated CH<sub>3</sub>CHOO Criegee intermediates to OH radical products. *Nat. Chem.* **2016**, *8* (5), 509-514.
- 20. Kroll, J. H.; Clarke, J. S.; Donahue, N. M.; Anderson, J. G.; Demerjian, K. L., Mechanism of HOx formation in the gas-phase ozone-alkene reaction. 1. Direct, pressure-dependent measurements of prompt OH yields. *J. Phys. Chem. A* **2001**, *105* (9), 1554-1560.
- 21. Kroll, J. H.; Sahay, S. R.; Anderson, J. G.; Demerjian, K. L.; Donahue, N. M., Mechanism of HOx formation in the gas-phase ozone-alkene reaction. 2. Prompt versus thermal dissociation of carbonyl oxides to form OH. *J. Phys. Chem. A* **2001**, *105* (18), 4446-4457.
- 22. Barber, V. P.; Hansen, A. S.; Georgievskii, Y.; Klippenstein, S. J.; Lester, M. I., Experimental and theoretical studies of the doubly substituted methyl-ethyl Criegee intermediate: Infrared action spectroscopy and unimolecular decay to OH radical products. *J. Chem. Phys.* **2020**, *152* (9), 094301.
- 23. Vereecken, L.; Novelli, A.; Taraborrelli, D., Unimolecular decay strongly limits the atmospheric impact of Criegee intermediates. *Phys. Chem. Chem. Phys.* **2017**, *19* (47), 31599-31612.
- 24. Cabezas, C.; Guillemin, J.-C.; Endo, Y., Probing the conformational behavior of the doubly substituted methyl-ethyl Criegee intermediate by FTMW spectroscopy. *J. Chem. Phys.* **2017**, *146* (17), 174304.
- 25. Liu, T. L.; Zou, M. J.; Caracciolo, A.; Sojdak, C. A.; Lester, M. I., Substituent Effects on the Electronic Spectroscopy of Four-Carbon Criegee Intermediates. *J. Phys. Chem. A* **2022**, *126* (38), 6734-6741.
- 26. Osborn, D. L.; Zou, P.; Johnsen, H.; Hayden, C. C.; Taatjes, C. A.; Knyazev, V. D.; North, S. W.; Peterka, D. S.; Ahmed, M.; Leone, S. R., The multiplexed chemical kinetic photoionization mass spectrometer: A new approach to isomer-resolved chemical kinetics. *Rev. Sci. Instrum.* **2008**, *79* (10), 104103.
- 27. Pross, A.; Sternhell, S., Oxidation of hydrazones with iodine in the presence of base. *Aust. J. Chem.* **1970**, *23* (5), 989-1003.
- 28. Yaws, C. L.; Satyro, M. A., Chapter 1 Vapor Pressure Organic Compounds. In *The Yaws Handbook of Vapor Pressure (Second Edition)*, Yaws, C. L., Ed. Gulf Professional Publishing: 2015; pp 1-314.
- 29. Person, J. C.; Nicole, P. P., Isotope Effects in the Photoionization Yields and the Absorption Cross Sections for Acetylene, Propyne, and Propene. *J. Chem. Phys.* **1970**, *53* (5), 1767-1774.
- 30. Welz, O.; Zádor, J.; Savee, J. D.; Ng, M. Y.; Meloni, G.; Fernandes, R. X.; Sheps, L.; Simmons, B. A.; Lee, T. S.; Osborn, D. L.; Taatjes, C. A., Low-temperature combustion chemistry of biofuels: pathways in the initial low-temperature (550 K–750 K) oxidation chemistry of isopentanol. *Phys. Chem. Phys.* **2012**, *14* (9), 3112-3127.
- 31. Yang, B.; Wang, J.; Cool, T. A.; Hansen, N.; Skeen, S.; Osborn, D. L., Absolute photoionization cross-sections of some combustion intermediates. *Int. J. Mass Spectrom.* **2012**, *309*, 118-128.
- 32. Goulay, F.; Derakhshan, A.; Maher, E.; Trevitt, A. J.; Savee, J. D.; Scheer, A. M.; Osborn, D. L.; Taatjes, C. A., Formation of dimethylketene and methacrolein by reaction of the CH radical with acetone. *Phys. Chem. Chem. Phys.* **2013**, *15* (11), 4049-4058.
- 33. Dodson, L. G.; Shen, L.; Savee, J. D.; Eddingsaas, N. C.; Welz, O.; Taatjes, C. A.; Osborn, D. L.; Sander, S. P.; Okumura, M., VUV Photoionization Cross Sections of HO<sub>2</sub>, H<sub>2</sub>O<sub>2</sub>, and H<sub>2</sub>CO. *J. Phys. Chem. A* **2015**, *119* (8), 1279-1291.
- 34. Caravan, R. L.; Rotavera, B.; Papajak, E.; Antonov, I. O.; Ramasesha, K.; Zádor, J.; Osborn, D. L.; Taatjes, C. A., personal communication via email, **2023**.
- 35. Rosch, D.; Caravan, R. L.; Taatjes, C. A.; Au, K.; Almeida, R.; Osborn, D. L., Absolute Photoionization Cross Section of the Simplest Enol, Vinyl Alcohol. *J. Phys. Chem. A* **2021**, *125* (36), 7920-7928.
- 36. Gozem, S.; Krylov, A. I., The ezSpectra suite: An easy-to-use toolkit for spectroscopy modeling. *WIREs Comput. Mol. Sci.* **2022**, *12* (2), e1546.

- 37. Wojcik, P.; Gozem, S.; Mozhayskiy, V.; Krylov, A. I. <a href="http://iopenshell.usc.edu/downloads">http://iopenshell.usc.edu/downloads</a>, accessed 2022-07-01.
- 38. Chhantyal-Pun, R.; Welz, O.; Savee, J. D.; Eskola, A. J.; Lee, E. P. F.; Blacker, L.; Hill, H. R.; Ashcroft, M.; Khan, M. A. H.; Lloyd-Jones, G. C.; Evans, L.; Rotavera, B.; Huang, H.; Osborn, D. L.; Mok, D. K. W.; Dyke, J. M.; Shallcross, D. E.; Percival, C. J.; Orr-Ewing, A. J.; Taatjes, C. A., Direct Measurements of Unimolecular and Bimolecular Reaction Kinetics of the Criegee Intermediate (CH<sub>3</sub>)<sub>2</sub>COO. *J. Phys. Chem. A* **2017**, *121* (1), 4-15.
- 39. Welz, O.; Savee, J. D.; Osborn, D. L.; Vasu, S. S.; Percival, C. J.; Shallcross, D. E.; Taatjes, C. A., Direct Kinetic Measurements of Criegee Intermediate (CH<sub>2</sub>OO) Formed by Reaction of CH<sub>2</sub>I with O<sub>2</sub>. *Science* **2012**, *335* (6065), 204-207.
- 40. Taatjes, C. A.; Welz, O.; Eskola, A. J.; Savee, J. D.; Scheer, A. M.; Shallcross, D. E.; Rotavera, B.; Lee, E. P. F.; Dyke, J. M.; Mok, D. K. W.; Osborn, D. L.; Percival, C. J., Direct Measurements of Conformer-Dependent Reactivity of the Criegee Intermediate CH<sub>3</sub>CHOO. *Science* **2013**, *340* (6129), 177-180.
- 41. Zou, M.; Liu, T.; Vansco, M. F.; Sojdak, C. A.; Markus, C. R.; Almeida, R.; Au, K.; Sheps, L.; Osborn, D. L.; Winiberg, F. A. F.; Percival, C. J.; Taatjes, C. A.; Klippenstein, S. J.; Lester, M. I.; Caravan, R. L., Bimolecular reaction of methy-ethyl substituted Criegee intermediate with SO<sub>2</sub>, personal communication via email, **2023**.
- 42. Lias, S. G., "Ionization Energy Evaluation". In NIST Chemistry WebBook, NIST Standard Reference Database Number 69, Eds. Linstrom, P. J.; Mallard, W. G., National Institute of Standards and Technology, Gaithersburg MD, 20899, <a href="https://doi.org/10.18434/T4D303">https://doi.org/10.18434/T4D303</a>, (retrieved April 14, 2022).
- 43. Rotavera, B.; Savee, J. D.; Antonov, I. O.; Caravan, R. L.; Sheps, L.; Osborn, D. L.; Zador, J.; Taatjes, C. A., Influence of oxygenation in cyclic hydrocarbons on chain-termination reactions from R + O<sub>2</sub>: tetrahydropyran and cyclohexane. *Proc. Combust. Inst.* **2017**, *36* (1), 597-606.
- 44. Gans, B.; Mendes, L. A. V.; Boye-Peronne, S.; Douin, S.; Garcia, G.; Soldi-Lose, H.; de Miranda, B. K. C.; Alcaraz, C.; Carrasco, N.; Pernot, P.; Gauyacq, D., Determination of the Absolute Photoionization Cross Sections of CH<sub>3</sub> and I Produced from a Pyrolysis Source, by Combined Synchrotron and Vacuum Ultraviolet Laser Studies. *J. Phys. Chem. A* **2010**, *114* (9), 3237-3246.
- 45. Wiedmann, R. T.; Tonkyn, R. G.; White, M. G.; Wang, K. H.; Mckoy, V., Rotationally Resolved Threshold Photoelectron-Spectra of OH and OD. *J. Chem. Phys.* **1992**, *97* (2), 768-772.
- 46. Dodson, L. G.; Savee, J. D.; Gozem, S.; Shen, L. H.; Krylov, A. I.; Taatjes, C. A.; Osborn, D. L.; Okumura, M., Vacuum ultraviolet photoionization cross section of the hydroxyl radical. *J. Chem. Phys.* **2018**, *148* (18).
- 47. Drozd, G. T.; Kurten, T.; Donahue, N. M.; Lester, M. I., Unimolecular Decay of the Dimethyl-Substituted Criegee Intermediate in Alkene Ozonolysis: Decay Time Scales and the Importance of Tunneling. *J. Phys. Chem. A* **2017**, *121* (32), 6036-6045.
- 48. Klippenstein, S. J., Variational optimizations in the Rice-Ramsperger-Kassel-Marcus theory calculations for unimolecular dissociations with no reverse barrier. *J. Chem. Phys.* **1992,** *96* (1), 367-371.
- 49. Georgievskii, Y.; Klippenstein, S. J., Transition state theory for multichannel addition reactions: Multifaceted dividing surfaces. *J. Phys. Chem. A* **2003**, *107* (46), 9776-9781.
- 50. Truhlar, D. G.; Garrett, B. C.; Klippenstein, S. J., Current status of transition-state theory. *J. Phys. Chem.* **1996**, *100* (31), 12771-12800.
- 51. Klippenstein, S. J.; Miller, J. A., From the time-dependent, multiple-well master equation to phenomenological rate coefficients. *J. Phys. Chem. A* **2002**, *106* (40), 9267-9277.
- 52. Miller, J. A.; Klippenstein, S. J., Master equation methods in gas phase chemical kinetics. *J. Phys. Chem. A* **2006**, *110* (36), 10528-10544.
- 53. Donahue, N. M.; Drozd, G. T.; Epstein, S. A.; Presto, A. A.; Kroll, J. H., Adventures in ozoneland: down the rabbit-hole. *Phys. Chem. Chem. Phys.* **2011**, *13* (23), 10848-10857.
- 54. Drozd, G. T.; Kroll, J.; Donahue, N. M., 2,3-Dimethyl-2-butene (TME) Ozonolysis: Pressure Dependence of Stabilized Criegee Intermediates and Evidence of Stabilized Vinyl Hydroperoxides. *J. Phys. Chem. A* **2011**, *115* (2), 161-166.

55. Cox, R. A.; Ammann, M.; Crowley, J. N.; Herrmann, H.; Jenkin, M. E.; McNeill, V. F.; Mellouki, A.; Troe, J.; Wallington, T. J., Evaluated kinetic and photochemical data for atmospheric chemistry: Volume VII – Criegee intermediates. *Atmos. Chem. Phys.* **2020**, *20* (21), 13497-13519.
56. Liu, T.; Elliot, S. N.; Zou, M.; Vansco, M. F.; Sojdak, C. A.; Markus, C. R.; Almeida, R.; Au, K.; Sheps, L.; Osborn, D. L.; Percival, C. J.; Taatjes, C. A.; Caravan, R. L.; Klippenstein, S. J.; Lester, M. I. OH Roaming and Beyond in the Unimolecular Decay of the Methyl-Ethyl Substituted Criegee Intermediate: Observations and Predictions, Zenodo, **2023**; <a href="https://zenodo.org/record/7839610#.ZD4xN-zMKzs">https://zenodo.org/record/7839610#.ZD4xN-zMKzs</a>.



TOC graphic